NATIONAL ADVISORY COMMITTEE
FOR AERONAUTICS

TECHNICAL NOTE 2742

BOUNDARY-LAYER DEVELOPMENT AND SKIN FRICTION

AT MACH NUMBER 3.05

By Paul F. Brinich and Nick S. Diaconis

Lewis Flight Propulsion Laboratory
Cleveland, Ohio

NACA

Washington

July 1952

NATIONAL ADVISORY COMMITTEE FOR AERONAUTICS

TECHNICAL NOTE 2742

BOUNDARY-LAYER DEVELOPMENT AND SKIN FRICTION AT MACH NUMBER 3.05

By Paul F. Brinich and Nick S. Diaconis

SUMMARY

Boundary-layer studies consisting of schlieren observations and momentum surveys were made on hollow cylinder models with their axes alined parallel to the stream. Results were obtained for three model diameters and for natural and artificially induced turbulent boundary-layer flows.

Transition Reynolds numbers were found to decrease with decreases in leading-edge thickness and with reductions in tunnel pressure level. Turbulent temperature-recovery factors generally decreased with increasing Reynolds number and were a maximum for the smallest transition Reynolds numbers.

The results of this investigation appeared to be consistent with the theoretical turbulent friction formulas of Wilson and with the extended Frankl-Voishel analysis of Rubesin, Maydew, and Varga. Velocity profiles in the outer portion of the boundary layer could be approximated reasonably with a 1/7 power profile and were found to be approximately similar in this region. Velocity profiles given by the Kármán universal turbulent boundary-layer profile parameters were found to be similar in the laminar sublayer and in the turbulent region.

INTRODUCTION

Total-pressure surveys of the turbulent boundary layer at supersonic speeds are made and analyzed in references 1, 2, and 3 for the purpose of determining skin-friction coefficients as a function of Reynolds number. Results of an investigation of a flat plate model spanning the tunnel are reported in reference 1. Turbulent boundary layers were formed by the natural transition from laminar to turbulent flow and surveys were made at several positions along the model length. The Mach number of the stream was varied from 1.70 to 2.19 and the tunnel was operated at a constant stagnation pressure at each Mach number, giving a maximum Reynolds number of about 22×10^6 for the turbulent boundary layer. To obtain the results given in reference 3, a smaller flat plate model was used and turbulent boundary layers were formed by the rapid

artificial transition to turbulent flow. A maximum Reynolds number of 1.1×10^6 was attained. The stream Mach number was 2.5 and the stagnation pressures were 30 and 40 pounds per square inch absolute.

Integrated friction coefficients were obtained in reference 1 by equating the measured momentum defects to the drag and making suitable corrections to the length of turbulent run because of the presence of the laminar boundary layer upstream. In reference 3 corrections to the length of run were necessary because of the high initial thickness of the boundary layer near the leading edge caused by the coating used to promote early transition to turbulent flow.

The present investigation, which was made at the NACA Lewis laboratory, is an extension of the aforementioned experimental investigations to a higher Mach number and contains a more detailed investigation of the effect of Reynolds number variation on the boundary-layer development and skin-friction coefficient. The conventional flat plates of references 1 and 3 were replaced by hollow cylinders with axes alined parallel to the stream direction. It was believed that the flow over the cylinders would be less subject to disturbing influences caused by the thick tunnel side-wall boundary layers than the conventional flat test plate mounted from the two tunnel side walls. In order to determine whether the boundary layer developed in the same manner as on a flat plate, boundary-layer measurements were made on three cylinders having different diameters.

Tests were conducted at a stream Mach number of about 3.05 and at stagnation pressures from 7 to 50 pounds per square inch absolute. This range of pressure permitted a Reynolds number variation from about 1 to 8×10^6 per foot, or a maximum Reynolds number of 14×10^6.

Each of the three models was tested with natural and artificial transition to turbulent boundary-layer flow to determine in what respect the two types of development are similar and whether it is possible to obtain a correlation of turbulent skin-friction coefficients from artifically turbulent boundary layers.

The analysis of the experimental results is made in a manner similar to that indicated in references 1 and 3 and, in addition, includes the measurement of the local skin-friction coefficient and a determination of the shape of the boundary-layer profile in terms of the Kármán similarity parameters for turbulent boundary-layer flow.

APPARATUS

The three basic cylinder models used in this investigation are shown in figure 1 together with pertinent dimensions. The addition of

roughness near the leading edge on each of these models gave a total of
six configurations tested. The models were 3, 4, and 5 inches in outside
diameter and 31 inches in length. The steel models were turned, ground,
and polished, and the leading edges were hardened to maintain their
sharpness. A single strut was provided for mounting the cylinders on the
tunnel side wall. Figure 2 shows a sketch of the 5-inch model in the
tunnel and the instrumentation setup for surveying the boundary layer.
The tunnel used for testing the model was the 1- by 1-foot variable
Reynolds number tunnel, which is a nonreturn type having a stagnation
pressure range of 5 to 52 pounds per square inch absolute.

Static-pressure orifices were provided along four lines on the top,
bottom, and two sides of the models. Spacing between orifices was
3 inches on the probing side, and 6 inches on the top, bottom, and
opposite side. Additional instrumentation was provided outside and
inside the lip in some cases. Four insulated thermocouples were imbedded
in the outside surface of the 5-inch cylinder just below the line of
static-pressure orifices on the survey side of the model at distances of
3, $6\frac{1}{2}$, $12\frac{1}{2}$, and $18\frac{1}{2}$ inches from the leading edge.

The roughness used to cause early transition from laminar to turbu-
lent flow consisted of a single layer of number 60 carborundum grit
applied in a clear lacquer coating in the form of a band extending from
the leading edge to 1/2 inch downstream. The coating had a decreased
density near the leading edge to minimize its effective bluntness.

The conventional boundary-layer-type total-pressure probes used were
made of 0.030- by 0.002-inch stainless-steel tubing flattened at the end
to 0.006-inch thickness with a 0.002-inch-high opening. These probes are
shown in figure 3. Probe (a) was used on the survey side of the model
and was 3 inches long from tip to heel; probes (b) and (c) were used on
the top and bottom of the model and were 4 inches long. Probe (a) was
translated by a mechanism which had a ±0.0005-inch positioning accuracy.
The average positioning accuracy relative to the model was about
±0.002 inch. Probes (b) and (c) were rotated by a mechanism having a
comparable positioning accuracy. Total pressures were measured on mercury
manometers and static pressures, on differential butyl phthalate manometers.

PROCEDURE

Before making boundary-layer measurements on the three models,
adjustments in angle of yaw and attack were made to minimize the differ-
ences of static pressure on opposite sides of the model. In each case the
final adjustment of the model, which amounted to yawing it a maximum of
$1/2°$ from the tunnel center line, yielded a pressure distribution in
which opposite orifices had maximum pressure differences of about
3 percent. After proper alinement of the model had been achieved, static-
pressure distributions were obtained at stagnation pressures of 7, 12, 20,
30, 40, and 50 pounds per square inch absolute for each of the three

models. Likewise, schlieren photographs were obtained to show the
leading-edge shock formation and the boundary-layer development. For
the 5-inch model, surface temperature measurements were made throughout
the pressure range. The stagnation temperature was approximately constant
at 50° F with a mean variation of 5° F and the dew point was kept below
-40° F.

Total-pressure boundary-layer surveys were made at eight positions
along the model 3 inches apart, starting 0.5 inch from the leading edge
and extending 21.5 inches back. The stagnation pressures at which these
surveys were made are indicated for each of the models in the following
table:

Model diameter (in.)	Tunnel stagnation pressure (lb/sq in. abs)	
	Natural transition	Artificial transition
3	12, 50	12
4	12, 50	12
5	7, 12, 20, 30, 50	7, 12, 20, 30, 50

Additional check measurements on the top and bottom of the model were
obtained to find whether the boundary-layer development about the model
was symmetrical. All surveys were made after the model surface tempera-
tures and pressures had reached equilibrium.

Reduction of Pressure Survey Data

The first step in computing the various boundary-layer quantities
used in the following analysis was to obtain the boundary-layer Mach
number distributions using the total-pressure surveys and model surface
static pressures. This was done by making the conventional assumption
of a constant static pressure within the boundary layer normal to the
surface and using the Rayleigh relation for a supersonic pitot tube.
Because the external and internal flow Mach numbers did not differ
greatly, it could be inferred that the flow over the cylinder is adiabatic
and that the assumption of constant total temperature throughout the
boundary layer is reasonable. With this assumption, velocity profiles
were computed from the Mach number profiles using the expression

$$\frac{u}{u_1} = \frac{M}{M_1} \sqrt{\frac{1 + \frac{\gamma-1}{2} M_1^2}{1 + \frac{\gamma-1}{2} M^2}}$$

(All symbols used in this report are listed in the appendix.) Two-
dimensional boundary-layer displacement thicknesses δ^* were computed by
the equation

$$\delta^* = \int_0^\delta \left(1 - \frac{\rho u}{\rho_1 u_1}\right) dy$$

and the corresponding momentum thickness θ, by

$$\theta = \int_0^\delta \frac{\rho u}{\rho_1 u_1} \left(1 - \frac{u}{u_1}\right) dy$$

where

$$\frac{\rho}{\rho_1} = \frac{1 + \frac{\gamma-1}{2} M^2}{1 + \frac{\gamma-1}{2} M_1^2}$$

A more precise calculation of the momentum thickness, taking into account the cylindrical form of the model, was made using the equation (reference 4)

$$\Theta = \theta + \frac{1}{r} \int_0^\delta \frac{\rho u}{\rho_1 u_1} \left(1 - \frac{u}{u_1}\right) y \, dy$$

where r is the radius of the cylinder. The contribution of the second term on the right side was a maximum of 14 percent for positions farthest downstream.

Although heat-transfer effects were assumed negligible, there still remains a question concerning the error resulting from assuming the total-temperature distribution in the boundary layer to be a constant. It is shown in reference 1 that this assumption has very little effect on the velocity or on the displacement and momentum thicknesses of turbulent profiles at Mach number 2. To check the validity of this assumption at a Mach number of 3.05, temperature distribution calculations based on the theory of reference 5 were made for four typical turbulent profiles using actual velocity profiles and observed wall temperature data. The maximum change in velocity from that obtained for the case of constant total temperature was $+2\frac{1}{2}$ percent, and the average changes in displacement and momentum thicknesses were -0.3 and -2 percent, respectively.

In general, both the skin-friction coefficient and the Reynolds number used in an experimental correlation of the same must be based on some value of the dynamic pressure which is representative of the free-stream value. Such values of the dynamic pressure were obtained from an

arithmetic average of the free-stream Mach number along the cylinder.
Because the friction coefficients (which also depend on the momentum
thicknesses) were calculated assuming a zero pressure gradient, the
observed momentum thickness had to be corrected for small deviations in
Mach number from the arithmetic average obtained along the model. The
method for making such corrections is given in reference 1 and was applied
to the measured velocity profiles to obtain corrected values of momentum
thickness. The maximum correction of the momentum thickness did not
exceed 2 percent. All the values of momentum thickness, friction coef-
ficient, and Reynolds number shown in the figures were corrected according
to the preceding scheme.

<div style="text-align:center">Accuracy of Pressure Measurements</div>

Total-pressure measurements in the boundary layer were estimated to
be accurate to ± 0.03 inch of mercury and static pressures, to ± 0.05 inch
of butyl phthalate. These limitations resulted in average Mach number
errors of ± 0.03 for the lowest tunnel pressure level tests; higher pres-
sures, of course, resulted in greater accuracy.

In computing the velocity profiles, the effective center of the
pitot tube was taken as its geometric center, and the edge of the boundary
layer was selected as the point where the velocity equaled about 99.9 per-
cent of the free-stream velocity. Probable errors in computing momentum
thickness based on the given accuracy in Mach number and the inherent
accuracy of the probe positioning device were approximately ± 1.5 percent.

The determination of the slope $d\Theta/dx$ which was used to find the
local friction coefficient was subject to large uncertainties because
of the great latitude within which a fairing of the experimental points
could be drawn. The probable error due to this fairing was estimated at
± 10 percent.

<div style="text-align:center">RESULTS AND DISCUSSION</div>

The ultimate purpose of this investigation is to correlate the skin-
friction coefficients obtained from momentum surveys with the Reynolds
number. Before this correlation can be made, however, several factors
must be considered to determine whether the conditions of the experiment
sufficiently approximate the assumptions of the theories with which the
experimental results are to be compared. These factors are: the degree
to which the actual pressure or Mach number gradient along the model
approximates the zero gradient, the determination of the laminar and
turbulent flow regions, the effect of the leading edge on the initial
boundary-layer development, the consistency of the measured wall
temperature-recovery factor with the assumption of zero heat transfer,
and the effect of cylinder diameter on the boundary-layer development.

Longitudinal Mach Number and Pressure Distributions

The longitudinal Mach number distributions for the 3-, 4-, and 5-inch
models with natural and artificial transition are shown in figures 4(a),
(b), and (c), respectively, at the various stagnation pressures. Mach
numbers were obtained from probe total-pressure and model static-pressure
data; most of the measurements were made along the side of the model.

The Mach number along the model generally increases from slightly
downstream of the leading edge to x = 15.5 inches; thereafter it drops
to lower values farther downstream. According to the momentum equation,
these changes in Mach number would cause errors in the value of the local
friction coefficient computed on the basis of a zero Mach number gradient.
These gradients introduce maximum errors of about 2 percent for x less
than 15.5 inches and 10 percent for x greater than 15.5 inches on the
5-inch model having artificial transition, which represents the worst
case.

A comparison of points on the top, bottom, and side of the model at
equal distances from the leading edge reveals slightly higher Mach numbers
and hence lower static pressures on the top and bottom of the model than
on the side. Schlieren observation showed no stream disturbances, such
as shock waves, which would cause such consistent variations in observed
pressure. The existence of such disturbances is not precluded, however,
since schlieren observations along a vertical light path, that is, through
the top and bottom of the tunnel, were impossible. It is believed that
the resulting pressure gradients around the body may cause secondary flows
which would transport low energy air to the top and bottom of the model,
giving more pronounced boundary-layer developments there.

Schlieren Observations

Typical schlieren photographs of the flow past the 5-inch model at
a stagnation pressure of 50 pounds per square inch absolute are shown in
figure 5(a) for natural transition and in figure 5(b) for artificial
transition. No tunnel stream shock waves are visible, indicating uniform
flow in vertical planes parallel to the flow. The starting shock of the
cylinder appears to be completely swallowed as indicated by the thin,
almost straight, attached leading-edge shock. (Additional static-pressure
instrumentation on the model interior indicated an internal Mach number
of 2.8.) Hundreds of 6-microsecond duration flash schlieren photographs
were taken, none of which showed evidence of high frequency intermittent
spillage or shock oscillation at the leading edge.

The leading-edge shock for the artificial transition is stronger
and steeper than for the natural transition, and is followed by an
expansion region at the end of the leading-edge roughness. A second
shock follows this region. The reflection location of the leading-edge

shock from the tunnel wall back to the model depends primarily on the
model diameter. The distances from the leading edge where the reflected
shock intersected the model are listed in the following table (no
schlieren data were available for the 3- and 4-in. models with artificial
transition):

Model		Distance from leading edge x (in.)
Natural transition	Artificial transition	
5-in.		19.2
4-in.		22.1
3-in.		24.6
	5-in.	18.3

A comparison of the longitudinal Mach number distributions of figures 4(a),
(b), and (c) and the respective distances in the preceding table shows
that only the 5-inch model experiences significant effects on Mach number
distribution due to the reflected leading-edge shock.

Data previously taken at the Lewis laboratory have shown that the
transition from laminar to turbulent flow observed by the schlieren
method can be correlated with the transition point obtained with pitot
surveys. The schlieren method has been used in the present investigation,
and figure 5(a) is a typical example of the appearance of the transition
region. The position of the transition point varied with time; this
fluctuation was observed by taking a large number of flash schlieren
photographs. The extreme fluctuations of position were about 1 inch
upstream and downstream of a given mean position. In figure 5(a) the
transition locations on the top and bottom were about equal, but in some
cases considerable differences in location were observed. An investiga-
tion was also made to determine whether there was any hysteresis lag in
the position of the transition point, particularly in going from one
pressure level to another. None was detected.

A plot of the transition Reynolds number based on the mean location
of the transition point is given as a function of the leading-edge thick-
ness for each of the various stagnation pressures in figure 6. The
transition location is the average of the mean locations on the top and
the bottom of the model as obtained from schlieren photographs. The model
diameters corresponding to the four leading-edge thicknesses are indicated.

Two sets of data appear for the 4-inch model, corresponding to two
thicknesses of the leading edge. In the beginning of the test program
it was suspected that the sharpness of the leading edge may be an impor-
tant factor in determining the boundary-layer development, since unusually

2451

large boundary-layer thicknesses were measured near the leading edge.
Accordingly, the leading-edge thickness was reduced from the initial
0.012-inch thickness to 0.002 inch by boring the inside of the lip;
considerably reduced boundary-layer thicknesses were then measured.
Figure 6 shows that the transition Reynolds numbers varied considerably
for these two leading-edge thicknesses, being much greater for the large
than for the small thickness. Data for the 3- and 5-inch models (which
had intermediate leading-edge thicknesses) are seen to fall between the
data for the two 4-inch-model leading edges, indicating a probable neg-
ligible dependence of the transition Reynolds number on the model diameter.

A very large dependence of the transition Reynolds number on the
tunnel stagnation pressure is indicated in figure 6. Changes in stagnation
pressure from 7 to 40 pounds per square inch absolute yielded 2.2 increases
in transition Reynolds number for each leading-edge thickness. The maximum
total change in transition Reynolds number obtained by varying both leading-
edge thickness and stagnation pressure is from 1.0 to 3.5×10^6. Presumably
still larger values could be obtained by increasing the leading-edge
thickness above 0.012 inch.

The decreased transition Reynolds numbers observed at the low stagna-
tion pressures are believed to be caused by the increased throttling in
the air supply to the tunnel plenum chamber required to attain the lower
stagnation pressures. Measurements of the instantaneous pressures in
the plenum chamber with a Statham pressure transducer indicated that the
maximum fluctuations in pressure were approximately equal at all stagna-
tion pressures. Hence, the turbulence level, expressed as the ratio of
pressure fluctuation to total pressure, increased for decreases in tunnel
stagnation pressure. The magnitude of the maximum fluctuation was about
0.8 inch of mercury.

<center>Temperature-Recovery Factor</center>

Temperature-recovery factors were computed from measurements of
the wall temperature on the 5-inch model having natural and artificial
transition in order to check the validity of the assumption of zero
heat transfer made in the calculation of the experimental velocity and
density distributions. These recovery factors are defined by

$$R = \frac{T_w - T_1}{T_0 - T_1}$$

and are shown plotted against Reynolds number in figure 7 for the full
range of stagnation pressure.

An examination of the recovery factors obtained for the case of natural transition shows an intial increase up to the transition point ($Re_{x_T} = 1.0 \times 10^6$ to 2.3×10^6 from fig. 6) and a gradual decrease thereafter in the turbulent region. This trend agrees with the experimental results of reference 6 to within 1 percent on the recovery factor, but the results of reference 7 are about 6 percent higher. The spread in the values of the recovery factor in the region $1 \times 10^6 < Re_x < 3 \times 10^6$ appears to be related to the different transition Reynolds numbers observed at the various pressures in figure 6. Thus the high recovery factors noted for the runs with 7, 12, and 20 pounds per square inch absolute stagnation pressure are associated with the relatively early transition to turbulent flow. The runs with 30 and 50 pounds per square inch pressure, which had higher transition Reynolds numbers, had notably lower recovery factors.

All the artificial transition recovery factors shown in figure 7 are for turbulent boundary layers. At Reynolds numbers from 2 to 12×10^6 these recovery factors agree fairly well with those obtained for natural transition flows. Below a Reynolds number of 2×10^6 they continue to increase above the values attained at the high Reynolds numbers and above the values shown for the laminar boundary-layer flow. Similar observations were made in reference 5 for the flow over a flat plate at a Mach number of 2.4.

The theoretical turbulent recovery factors of reference 5 for a Mach number of 3.05 are about 4 percent lower than the results obtained in this investigation.

Effect of Model Diameter and Leading-Edge

Thickness on Boundary-Layer Development

Measurements were made on three models of different diameters to determine the variation of boundary-layer development with surface curvature transverse to the flow. It was hoped that the trends observed for the various diameter models could be extrapolated to establish a relation for the boundary-layer development on a flat plate. However, the very great dependence of the boundary-layer development on the thickness of the leading edge, which varied from one model to another, precluded even a qualitative estimate of the effect of model diameter on the boundary-layer development.

Figures 8(a) and 8(b) show the variation of momentum thickness as a function of the leading-edge thickness for stagnation pressures of 12 and 50 pounds per square inch absolute and natural transition. Near the leading edges where the flows are predominately laminar the momentum thicknesses are largest for the 0.006-inch and least for the 0.003- and 0.002-inch leading edges. Farther downstream in the turbulent region

the reverse trend is apparent. A comparison of the momentum thicknesses at $x = 21.5$ inches for the various leading edges shows that reductions in momentum thickness of 10 to 20 percent are possible by blunting the leading edge from 0.002 to 0.006 inch. Presumably larger reductions in drag would be indicated by data from the 4-inch model having the 0.012-inch leading edge if such data were available.

The artificial transition results of figure 8(c) were obtained for turbulent boundary layers and indicate decreasing momentum thicknesses for thicker leading edges. Although the trends for the artificial transition data followed those for the natural transition in the turbulent region, the distributions of momentum thickness along the model were very irregular.

Because it is impossible to establish a relation between the cylinder and flat-plate boundary-layer developments from the experimental results, some alternate approach must be employed to justify the comparisons to be made between cylinder and flat-plate turbulent friction coefficients. If the relation between the turbulent friction coefficients for a cylinder and a flat plate may be assumed approximately similar to the relation between the laminar friction coefficients, then such a comparison may be justifiable. Theoretical calculations of the incompressible laminar friction coefficients made for the 3-inch cylinder model using the analysis of reference 8 show a maximum increase of 2 percent over those for a flat plate at a stagnation pressure of 12 pounds per square inch absolute, indicating that the comparisons to be made herein are probably valid.

Comparison of Experimental and Theoretical Laminar Velocity Profiles

Laminar-type velocity profiles were observed on all the models having natural transition at Reynolds numbers less than the transitional values indicated on figure 6, and on the 5-inch model having artificial transition at a stagnation pressure of 7 pounds per square inch absolute for the positions 0.5, 3.5, and 6.5 inches from the leading edge. Figure 9 shows the experimental laminar profiles obtained with natural transition on the side of the 5-inch model with the 0.003-inch leading-edge thickness and on the 4-inch model with the 0.012-inch leading-edge thickness. The theoretical dimensionless velocity and distance parameters of reference 9 have been used to present the experimental data, and the theoretical curve for $M = 3.05$ has been included for comparison.

The first observation to be made in figure 9 is that almost all the experimental points fall to the right of the theoretical line, indicating a more rapid boundary-layer development than that predicted by theory. That this greater initial growth is dependent on the thickness of the leading edge can be seen by comparing the two profiles obtained on the 4-inch model with the 0.012-inch leading edge at the 0.5-inch position with those obtained on the 5-inch model having a 0.003-inch leading edge.

This comparison of two different diameter models is justified because the 5-inch model had the same boundary-layer profile near the leading edge as the 4-inch model with the 0.002-inch leading edge. The 0.012-inch leading edge gives boundary layers far thicker than the 0.003-inch edge. In addition, the boundary layers with the 0.003-inch edge have an inflection in the profile near the free-stream edge of the boundary layer which gives boundary-layer velocities in excess of stream velocities by as much as 3 percent. From the results concerning transition discussed earlier, the generalization may be made that the thicker leading edge gives thicker initial boundary layers and larger transition Reynolds numbers than the thin leading edge. Further, the appearance of the velocities in excess of the free-stream value in the profile is associated with a decrease in the transition Reynolds number. This latter point was more firmly established for the 3-inch model in which the excess velocity in the profile was almost indiscernible and the transition Reynolds number was substantially higher than for the other models having larger excess velocities. The excess velocity regions shown in figure 9 are not particularly impressive when shown in terms of u/u_1 but become very substantial in the indicated pitot pressure surveys. These regions were detected as far downstream as 3.5 inches; they diminish in intensity as distance increases.

A further comparison of experiment and theory in figure 9 shows that discrepancies diminish with increasing distance downstream and with decreasing total pressures. The diminution with distance is to be expected since the effect is associated with the leading edge. The thinnest leading edges gave the best agreement with theory.

A possible reason for the poor agreement between the experimental measurements and theory in the region near the leading edge may be that the large probe size relative to the boundary-layer thickness made it impossible to obtain accurate, undisturbed boundary-layer measurements. However, the changes in shape of the measured profiles corresponding to small changes in leading-edge thickness were associated with changes in transition location as noted in schlieren photographs. For this reason it must be concluded that the probes are sufficiently sensitive to detect qualitative changes in profile caused by independent variations, such as changes in the leading-edge thickness.

Another possible source of error arose from vibrations of the models, which were strongest over the forward portion and at high stagnation pressures. These vibrations resulted from the long cantilever mounting from the single support strut at the rear and may contribute slightly to the measured boundary-layer thickness over the forward portion of the model. The turbulent profiles are not believed to be noticeably affected by this vibration.

Turbulent Velocity Profiles and Friction Coefficients

Two methods for studying similarity among turbulent velocity profiles are in common usage. In the first method the various turbulent velocity profiles are expressed in terms of the nondimensional velocity u/u_1 and distance y/δ or y/Θ. This method has been used in the analysis of incompressible and compressible flow boundary layers and is usually considered to apply only to the outer part of the turbulent boundary layer. In the second method the similarity parameters are the nondimensional friction velocity ratio $u/\sqrt{\tau_0/\rho}$ and the friction distance parameter $(\rho\sqrt{\tau_0/\rho})(y/\mu)$. These parameters define the Kármán universal turbulent logarithmic velocity profile which follows from the turbulent mixing length theory. This method has been used extensively for the analysis of subsonic turbulent boundary-layer data, both incompressible and compressible (e.g., references 10 and 11); however, its application to supersonic turbulent boundary-layer data is almost unknown. Both these methods will be used to analyze the boundary layers measured in this investigation and to determine their range of application.

The subject of greatest practical interest here, however, is the determination of the friction coefficient over the widest possible range of Reynolds number. Two procedures for presenting skin friction data are commonly used. The first procedure relates the integrated flat-plate friction coefficient C_f to the Reynolds number based on length of run Re_x where C_f is determined from

$$C_f = \frac{2\Theta}{x}$$

This method will be used to present friction coefficient results for both natural and artificial transition boundary layers. Since for the case of natural transition a part of the measured momentum thickness Θ and the length of run x or both may be thought of as due to the upstream laminar layer, the turbulent friction coefficient C_f as defined will be incorrect and result in low values of the coefficient. Hence, a correction equivalent to increasing the momentum thickness Θ or decreasing the length of run x or both is necessary to obtain a friction coefficient for comparison with empirical formulas for turbulent two-dimensional flow. Such corrections can be made with low-speed empirical friction laws as guides.

In the second procedure the local friction coefficient c_f is related to the Reynolds number based on momentum thickness Re_Θ. This method requires no correction to the momentum thickness or length of run since the relation between c_f and Re_Θ is generally believed to be fairly independent of the previous history of the boundary layer and the location

of the transition point. The validity of the two methods will then be
investigated by comparing the results obtained from each.

Turbulent velocity profiles u/u_1 versus y/Θ. - Turbulent velocity
profiles u/u_1 against y/Θ are plotted in figures 10(a) and 10(b) for
representative locations and pressures along the side of the 5-inch model
for both natural and artificial transition. These plots show approximate
similarity of the turbulent profiles whether produced naturally or arti-
ficially for values of $y/\Theta > 3.0$ and, when compared with the power
profiles indicated by the solid lines, show the closest agreement with
the 1/7 power law. The somewhat higher degree of similarity in the arti-
ficial transition plots for the region near the wall reflects the smaller
variation in Θ along the model length compared with that for the natural
transition.

Integrated friction coefficients. - In order to simplify the presen-
tation of the integrated friction coefficient data and to facilitate the
subsequent corrections to the momentum thickness and length of run neces-
sary to obtain coefficients for 100 percent turbulent flow, the friction
coefficient C_f has been expressed in terms of the Reynolds numbers
based on the momentum thickness and length of run

$$C_f = \frac{2\Theta}{x} = \frac{2\ Re_\Theta}{Re_x}$$

If it is assumed that the integrated friction coefficient can be expressed
in terms of the Reynolds number raised to a power as for incompressible
completely turbulent flow

$$C_f = \frac{K}{Re_x{}^n}$$

where K and n are constants, then substituting the former expres-
sion for C_f gives the following:

$$Re_\Theta = \frac{K}{2}\ (Re_x)^{1-n}$$

A plot of these variables Re_Θ and Re_x on log-log coordinates yields
a straight line, the slope of which is $1-n$.

All measurements of Re_Θ and Re_x for natural and artificial
transition on all models are plotted in figures 11(a) and 11(b). A
single line approximating the average distribution of the experimental

points has been faired in figure 11(a). This line is a curve concave
downward. If the requirement for purely turbulent flow that this line
be straight is to be satisfied, then a constant addition $\Delta Re_\Theta = 0.6 \times 10^3$
or a subtraction $\Delta Re_x = 0.6 \times 10^6$ or some combination of the two must be
made. Accordingly, such corrections to the original curve have been
made and are represented by the single dot-dash straight line of fig-
ure 11(a). Because the final curve has a slope so nearly equal to 1, a
correction involving ΔRe_Θ gives the same corrected line as a correction
involving ΔRe_x.

The corrected line may be represented by an equation given in terms
of the integrated friction coefficient

$$C_f = \frac{0.039}{Re_x^{0.19}}$$

or if a compressibility factor of the form $\left(1 + \frac{\gamma-1}{2} M_1^2\right)^m$ is separated
out and the constant 0.074 of the incompressible law is assumed correct,

$$C_f = \frac{0.074}{Re_x^{0.19}} \left(1 + \frac{\gamma-1}{2} M_1^2\right)^{-0.6}$$

The friction coefficient formulas of von Kármán (reference 12), of Wilson
(reference 2), and of Rubesin, Maydew, and Varga in their extended Frankl
and Voishel analysis (reference 3) are shown in figure 11(a) all based on
the same linear temperature-viscosity relation. The formulas given by
references 2 and 3 are seen to best fit the corrected experimental data.

Strictly speaking, the method of applying these corrections is not
exact because the subtraction or addition of a constant amount ΔRe_x or
ΔRe_Θ, respectively, implies that the turbulent flow begins at the same
Reynolds number regardless of stagnation pressure or leading-edge thick-
ness. Figure 6 showed that, actually, the transition Reynolds number
varied over a wide range which was substantially higher than the value
of $\Delta Re_x = 0.6 \times 10^6$ used for one of the two possible corrections in fig-
ure 11(a). However, there is no reason why the apparent beginning of the
turbulent boundary layer $(\Delta Re_x = 0.6 \times 10^6)$ should correspond to the
actual beginning of it, for the former will have its origin in the transi-
tional layer immediately following the initial laminar layer.

Nevertheless, attempts were made to correct each set of data indi-
vidually so as to separate out the effects of a varying transition
Reynolds number. Because of extraneous effects, for example, possibly

those associated with the leading edge or secondary flows, some of the
individual sets of data exhibited some serious inconsistencies, such as
transition Reynolds numbers Re_{x_T} having negative values. Rather than
an attempt to rationalize these inconsistencies or to discard the irregular
data points, the procedure of including all the points in one plot of
Re_θ against Re_x was decided upon. The results obtained by this method
should then be understood to contain an average of all the results cor-
responding to some average transition Reynolds number.

The corresponding results for the models having artificial transition
are shown in figure 11(b), and it is to be noted that the experimental
points can no longer be approximated by a single curved line, but rather
are approximated by a family of curves - one for each pressure. The dot-
dash line shown is taken directly from figure 11(a) where it represented
the final correction of the original experimental results. In figure 11(b)
the experimental points fall to the left of the corrected line, neces-
sitating the opposite corrections, that is, a subtraction ΔRe_θ or

addition ΔRe_x. This time, however, a specific correction varying with
the pressure is required for the uncorrected experimental curves to
approximate the dashed line. Approximate corrections ΔRe_θ and ΔRe_x
are listed in the following table for the artificial turbulence flow on
all three models:

p_0 (lb/sq in. abs)	7	12	20	30	50
ΔRe_θ	0	-0.4×10^3	-0.8×10^3	-1.3×10^3	-2.7×10^3
ΔRe_x	0	$.4\times10^6$	$.8\times10^6$	1.5×10^6	3.5×10^6

Thus, very large corrections are indicated for the highest stagna-
tion pressures and negligible ones, for the lowest. This increased
discrepancy at high pressures appears to be analogous to the increased
discrepancy between experiment and theory in the case of the laminar
boundary layer (fig. 9) where the same behavior with pressure was noted.
Likewise, the greatest percentage deviations in the artificial turbulent
boundary-layer development expressed in terms of the momentum thickness
occurred near the leading edge, again comparable with the laminar boundary-
layer case where the poorest agreement between experiment and theory was
observed closest to the leading edge. The effect of adding roughness at
the leading edge is therefore to cause a disturbance which increases the
initial momentum thickness and which increases with the pressure or
density.

Local friction coefficients. - Because of the arbitrary nature of
the assumptions used to correct the measured values of Re_x and Re_θ

in order to obtain the relation between integrated friction coefficient
and Reynolds number, a different approach was tried which was expected
to eliminate the necessity of making corrections for the effective lead-
ing edge or effective momentum thickness. In this second method the
slope of the curve of momentum thickness against x, which is proportional
to the local friction coefficient for a flat plate, was correlated against
the Reynolds number based on the momentum thickness.

The curves of momentum thickness against x which were faired
through the experimental points are shown in figure 12. A careful examina-
tion of the experimental points shows that the momentum thickness on the
top and the bottom of the model was almost always larger than on the side.
For this reason the curves faired through the experimental points repre-
sent average values among the top, bottom, and side. These large dif-
ferences in boundary-layer development predominate in the turbulent region
and appear to be caused by differences in the location of the transition
point or by generally low static pressures on the top and the bottom of
the model. In the laminar region the development in the three circum-
ferential positions is very nearly equal.

The values of $d\Theta/dx$ and Re_Θ obtained with the aid of the faired
curves of figure 12 are shown plotted in figure 13. Also shown are the
semiempirical curves of Wilson (reference 2), of Rubesin, Maydew, and
Varga's extended Frankl and Voishel analysis (reference 3), and of
von Kármán (reference 12), and the laminar curve of Chapman and Rubesin
(reference 9), all with a linear temperature-viscosity relation. A
comparison in figure 13(a) of the experimental results and the theories
of references 2 and 3 shows good agreement up to $Re_\Theta = 5000$. Above
this value the experimental points show a general downward trend.

Figure 13(b) shows the local friction coefficient plot for artificial
transition together with the theoretical turbulent curves indicated in
figure 13(a). In this case there is little correlation between experiment
and theory. The discrepancy in the slopes of the data is greatest at the
high pressures and least at the low, which was a characteristic observed
to a certain extent for the natural transition results and also earlier
for the uncorrected plot of Re_Θ against Re_x for artificial transition
(fig. 11(b)).

In order to compare the friction coefficients obtained by the two
methods for both the natural and artificial transition, the equations
obtained from the results of figures 11(a) and 11(b) were converted to
the $d\Theta/dx$ against Re_Θ coordinate system of figure 13 and are presented
with the local friction coefficients in figure 14. Very good agreement
between the two methods is apparent for the natural transition up to
$Re_\Theta = 5000$. The artificial transition results show little correlation
throughout. These results show that fairly typical correlations of

turbulent friction coefficient with Reynolds number are possible without
resort to correction of any kind for the case of natural transition
boundary-layer flow. Such correlations are not possible for the case of
artificially turbulent flows.

Turbulent velocity profiles u^+ against y^+. - The Kármán similarity
parameters u^+ and y^+ are given by the following expressions; local
values of density and viscosity and wall values for the shear stress are
used:

$$u^+ = \frac{u}{\sqrt{\frac{\tau_0}{\rho}}} = \frac{u}{u_1} \sqrt{\frac{\rho}{\rho_1}} \sqrt{\frac{2}{c_f}}$$

$$y^+ = \frac{\rho y \sqrt{\frac{\tau_0}{\rho}}}{\mu} = \frac{u_1 y}{\nu} \sqrt{\frac{\rho_1}{\rho}} \sqrt{\frac{c_f}{2}}$$

The assumptions of a constant total temperature and a linear temperature-
viscosity relation were used in computing the quantities u^+ and y^+
by the following equations, which are related to the stagnation conditions
and the Mach number:

$$u^+ = \frac{M}{M_1} \sqrt{\frac{2}{c_f}}$$

$$y^+ = \frac{\sqrt{\gamma R T_0}}{\nu_0} M_1 \frac{\left(1 + \frac{\gamma-1}{2} M^2\right)^{\frac{2-\gamma}{\gamma-1}}}{\left(1 + \frac{\gamma-1}{2} M_1^2\right)^{\frac{\gamma}{\gamma-1}}} y \sqrt{\frac{c_f}{2}}$$

In order to compute these parameters it is necessary to know the
local coefficients c_f for each profile. These were obtained from the
experimental curves of figure 14. Each of the several determinations of
friction coefficient shown in figure 14 was tried to find which gave
similarity among the various profiles in the turbulent region nearest
the wall; the curve obtained from the plot of Re_θ against Re_x, where
corrections for the effective leading edge or momentum defect were made,
gave the most satisfactory results for both the natural and artificial
transition boundary layers. The curves obtained from the plot of $c_f/2$
against Re_θ for the artificial transition (fig. 13(b)) gave friction
coefficients which produced very large discrepancies among the various

profiles in the plot of u^+ against y^+. Therefore, if similarity of the turbulent profiles may be assumed a satisfactory criterion for judging which determination of the friction coefficient is most reliable, then it must be concluded that the results obtained by the correction method of figures 11(a) and 11(b) are the best.

Even when the friction coefficient results based on the correction method of figures 11(a) and 11(b) were used, a slight deviation from similarity was observed. This deviation was corrected to a mean line representative of all the profiles measured by adjusting the friction coefficient a constant amount for each individual profile, ± 5 percent on the average. The plots of u^+ against $\log y^+$ obtained with these corrections to the friction coefficient are shown in figures 15(a) and 15(b) for the same turbulent profiles presented earlier in figures 10(a) and 10(b), respectively. Good similarity is apparent throughout the entire range of values of u^+ and $\log y^+$ except near the outer edge of the boundary layer where the maximum value of u^+ is reached. The value of u^+ there is given by

$$u^+_{max} = \sqrt{\frac{2}{c_f}}$$

This value of u^+_{max} is probably not the true maximum value of u^+ at the edge of the boundary layer, because the shear stress there has been assumed equal to the wall value. Small reductions in the shear stress or friction coefficient near the edge of the boundary layer therefore could produce similarity throughout the entire boundary layer. The greater departure from similarity for the artificial transition boundary layer compared with the natural in the region near the stream edge is caused by increased mixing, which extends the velocity boundary layer into a region of relatively low shearing stress.

Included in figure 15 for comparison with the experimental results are the theoretical laminar sublayer and turbulent layer curves for incompressible flow from reference 10 and some theoretical turbulent layer curves for compressible flow computed from reference 11. Making due allowances for the rather poor accuracy in the laminar sublayer allows this portion of the experimental boundary layer to be easily distinguished and identified with the theoretical laminar sublayer curve.

The theoretical representation for incompressible turbulent flow is shown by the single straight line of reference 8. The equation of this line is

$$u^+ = 5.5 + \frac{1}{K} \log y^+$$

where $K = 0.40$ and is universal for all incompressible turbulent
boundary layers. The method used in reference 11 to determine the effect
of compressibility resulted in an expression for the compressible tur-
bulent region where u^+ is a function of both y^+ and the shear stress
or friction coefficient. Hence, the theoretical compressible turbulent
flow region will be represented by a family of lines depending on the
value of the shear stress assumed. The compressible turbulent curves
shown in figure 15 were computed by the method of reference 11 for a
stream Mach number of 3.05 and two typical values of the local friction
coefficient, 0.00144 and 0.00250. The constant K was taken as 0.40.

A comparison of the compressible flow theory with the experimental
results shows that the general theoretical trends are approximately
borne out by experiment. Somewhat better agreement between the two
could be obtained by further adjustment of the theoretical constant K
and of the integration constant in the expression of reference 11 for
the compressible turbulent flow region.

When the effect of compressibility is considered as in reference 11,
the theoretical profiles depend on the particular value of friction
coefficient chosen. The effect of differences in the assumed friction
coefficients is small near the wall and increases as the edge of the
boundary layer is approached, producing a distinct profile for each value
of the friction coefficient. The experimental friction coefficients
were modified so as to make the experimental profiles coincide in the
region of $\log y^+ = 1.7$, and similarity throughout almost the entire
boundary layer resulted. The agreement between experiment and theory in
the region of $\log y^+ = 1.7$ is found to be good, but as larger values of
$\log y^+$ are taken the agreement diminishes. The experimental points are
seen to form a universal curve throughout the boundary layer which agrees
with the theoretical curve only in the region near the wall. In the
outer region where each of the theoretical curves depends on the value
of the friction coefficient assumed, the agreement is poor.

Since small changes in the measured friction coefficient were
necessary to establish the similarity of the turbulent velocity profiles,
it is of interest to note what differences have been made in the curve
of $c_f/2$ against Re_θ originally taken from figure 14. In figure 16
are shown the original curve and the corrected values of the friction
coefficient necessary to establish similarity in figures 15(a) and 15(b).
Both the natural and artificially turbulent boundary-layer results are
shown and are seen to agree closely. The corrections to the original
curve did not exceed 10 percent. It thus appears that if the profiles
are made similar by adjustment of the local friction coefficients, then
these friction coefficients remain continuous and smooth functions of
Re_θ as they were before adjustment and a good correlation is obtained
both for natural and for artificial transition.

SUMMARY OF RESULTS

The following results were obtained from the investigation of the boundary-layer development in a zero pressure gradient at Mach number 3.05:

1. The position of transition varied with time, the extreme positions being about 1 inch upstream and downstream of a mean location.

2. The transition Reynolds number was found to increase for increasing stagnation pressures and for increasing leading-edge thicknesses. The maximum variation in transition Reynolds number was from 1.0 to 3.5×10^6.

3. Turbulent temperature recovery factors were found to decrease slightly with increasing Reynolds number. The largest values of the recovery factor were found for the initially turbulent region and increased with decreasing transition Reynolds number. Natural and artificial transition flows gave equal recoveries in the turbulent region for equal Reynolds numbers.

4. No distinct model diameter effect was found in the boundary-layer growth. If such an effect existed, it was obscured by slight variations in the leading-edge thickness for the different models. The thickness of the leading edge had a pronounced effect on the boundary-layer development.

5. The agreement between the experimental and theoretical laminar boundary-layer profiles was excellent for low stagnation pressures, large distances downstream of the leading edge, and small leading-edge radii. Possible errors due to the relatively large size of the probe compared with the boundary-layer thickness may have some effect on the quantitative results found nearest the leading edge, but the general trends observed are probably correct.

6. Naturally and artificially turbulent boundary-layer profiles of the dimensionless velocity and distance parameters, u/u_1 against y/θ, showed approximate similarity in the outer portion of the boundary layer, and the approximation to the power profile was best for a power profile exponent N equal to 7.

7. Integrated turbulent friction coefficients for natural and artificial transition were correlated against Reynolds number based on length of run by suitable corrections to account for transition and leading-edge effects. Good agreement with the theoretical friction coefficient formulas of Wilson and of Rubesin, Maydew, and Varga in their extended Frankl and Voishel analysis was obtained.

8. Local turbulent friction coefficients for natural and artificial transition were correlated against Reynolds number based on momentum thickness without making any corrections to account for transition and leading-edge effects. Good agreement with theory was obtained for the natural transition boundary layers up to a Reynolds number of 5000. Very poor agreement was found for the artificial transition boundary layers.

9. Naturally and artificially turbulent boundary-layer profiles expressed in terms of the Kármán turbulent profile velocity and distance parameters u^+ and $\log y^+$, respectively, showed similarity throughout the boundary layer except for the region nearest the stream edge. The departure from similarity was greatest for the artificial transition boundary layers and was probably caused by a more extended region of low shear turbulent mixing.

Lewis Flight Propulsion Laboratory
   National Advisory Committee for Aeronautics
      Cleveland, Ohio, April 10, 1952

APPENDIX - SYMBOLS

The following symbols are used in this report:

c   proportionality constant in viscosity-temperature relation given in reference 9

c_f local friction coefficient, $\tau_0 / \rho_1 u_1^2 / 2$

C_f integrated friction coefficient, friction $\mathrm{drag} / \rho_1 u_1^2 / 2$

m   exponent of compressibility factor

M   Mach number

M_1 stream Mach number

N   exponent in power profile relation, $\dfrac{u}{u_1} = \left(\dfrac{y}{\delta}\right)^{\frac{1}{N}}$

n   exponent of Reynolds number in friction formula

P_0 stagnation pressure

r   radius of model

R   temperature-recovery factor

Re_x Reynolds number based on length of run

Re_θ Reynolds number based on momentum thickness

Re_{x_T} Re_x of transition

T_1 stream static temperature

T_0 stream total temperature

T_w wall temperature

u   velocity

u_1 stream velocity

u^+ Kármán turbulent boundary-layer velocity parameter

x   distance along model from leading edge

y   distance normal to model

y^+ Kármán turbulent boundary-layer distance parameter

γ ratio of specific heat at constant pressure to specific heat at constant volume

δ boundary-layer thickness

δ^* two-dimensional displacement thickness

θ two-dimensional momentum thickness

Θ three-dimensional momentum thickness on cylindrical body

μ viscosity

ν kinematic viscosity

ρ density

ρ_1 stream density

τ_0 shear stress at wall

REFERENCES

1. Wilson, R. E., Young, E. C., and Thompson, M. J.: 2nd Interim Report on Experimentally Determined Turbulent Boundary Layer Characteristics at Supersonic Speeds. CM-501, DRL-196, Defense Res. Lab., Univ. Texas, Jan. 25, 1949. (Bur. Ord. Contract NOrd-9195.)

2. Wilson, R. E.: Turbulent Boundary Layer Characteristics at Supersonic Speeds - Theory and Experiment. CM-569, DRL-221, Defense Res. Lab., Univ. Texas, Nov. 21, 1949. (Bur. Ord. Contract NOrd-9195.)

3. Rubesin, Morris W., Maydew, Randall C., and Varga, Stevan A.: An Analytical and Experimental Investigation of the Skin Friction of the Turbulent Boundary Layer on a Flat Plate at Supersonic Speeds. NACA TN 2305, 1951.

4. Tetervin, Neal: Approximate Formulas for the Computation of Turbulent Boundary-Layer Momentum Thicknesses in Compressible Flows. NACA ACR L6A22, 1946.

5. Tucker, Maurice, and Maslen, Stephen H.: Turbulent Boundary-Layer Temperature Recovery Factors in Two-Dimensional Supersonic Flow. NACA TN 2296, 1951.

6. Staldter, Jackson R., Rubesin, Morris W., and Tendeland, Thorval: A Determination of the Laminar-, Transitional-, and Turbulent-Boundary-Layer Temperature-Recovery Factors on a Flat Plate in Supersonic Flow. NACA TN 2077, 1950.

7. Eber, G. R.: Recent·Investigation of Temperature Recovery and Heat Transmission on Cones and Cylinders in Axial Flow in the N.O.L. Aeroballistics Wind Tunnel? Jour. Aero. Sci., vol. 19, no. 1, Jan. 1952, pp. 1-6.

8. Seban, R. A., and Bond, R.: Skin-Friction and Heat-Transfer Characteristics of a Laminar Boundary Layer on a Cylinder in Axial Incompressible Flow. Jour. Aero. Sci., vol. 18, no. 10, Oct. 1951, pp. 671-675.

9. Chapman, Dean R., and Rubesin, Morris W.: Temperature and Velocity Profiles in the Compressible Laminar Boundary Layer with Arbitrary Distribution of Surface Temperature. Jour. Aero. Sci., vol. 16, no. 9, Sept. 1949, pp. 547-565.

10. von Kármán, Th.: Turbulence and Skin Friction. Jour. Aero. Sci., vol. 1, no. 1, Jan. 1934, pp. 1-20.

11. Deissler, Robert G.: Analytical and Experimental Investigation of Adiabatic Turbulent Flow in Smooth Tubes. NACA TN 2138, 1950.

12. de Kármán, Th.: The Problem of Resistance in Compressible Fluids. Quinto Convegno "Volta," Reale Accademia d'Italia (Roma), Sett. 30-Ott. 6, 1935, pp. 3-57.

2451

Boundary layers
measured here, 21.5"

31"

5°

d D

Surface polished to less
than 16 microinches rms
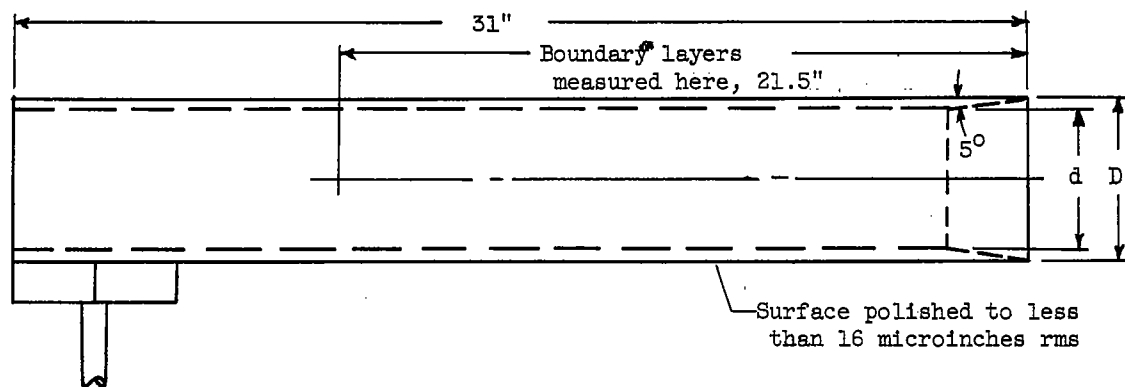
D (in.)	d (in.)	Leading-edge thickness (in.)
3	2.83	0.006
4	3.67	.012
4	3.67	.002
5	4.50	.003

Figure 1. - Cylinder model dimensions.

Air
flow

Top view

Front view
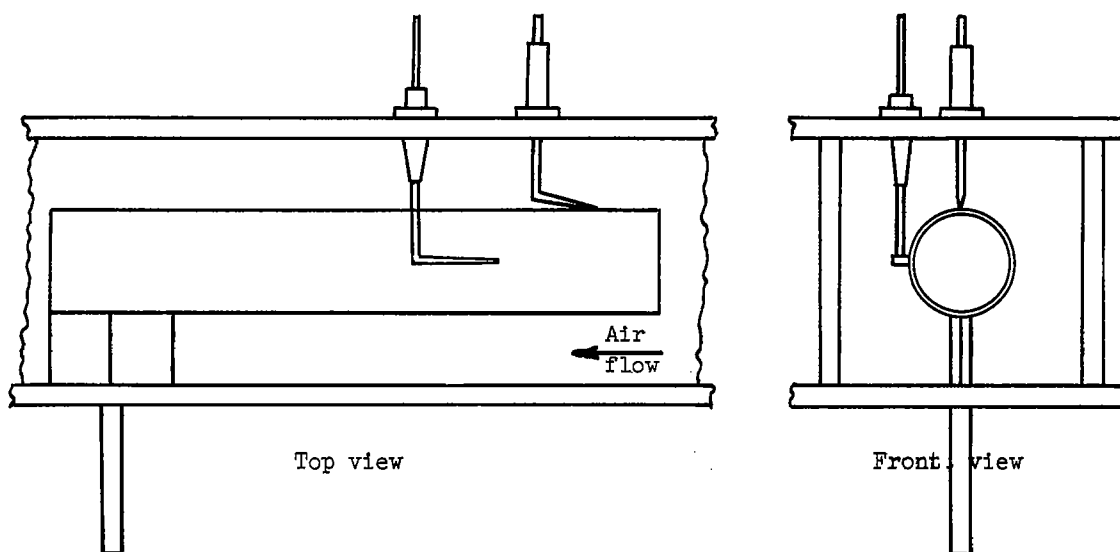
Figure 2. - Five-inch model in tunnel showing probe instrumentation.

(a) Side probe. (b) Top probe. (c) Bottom probe.

Figure 3. - Total-pressure probes used for boundary-layer surveys.
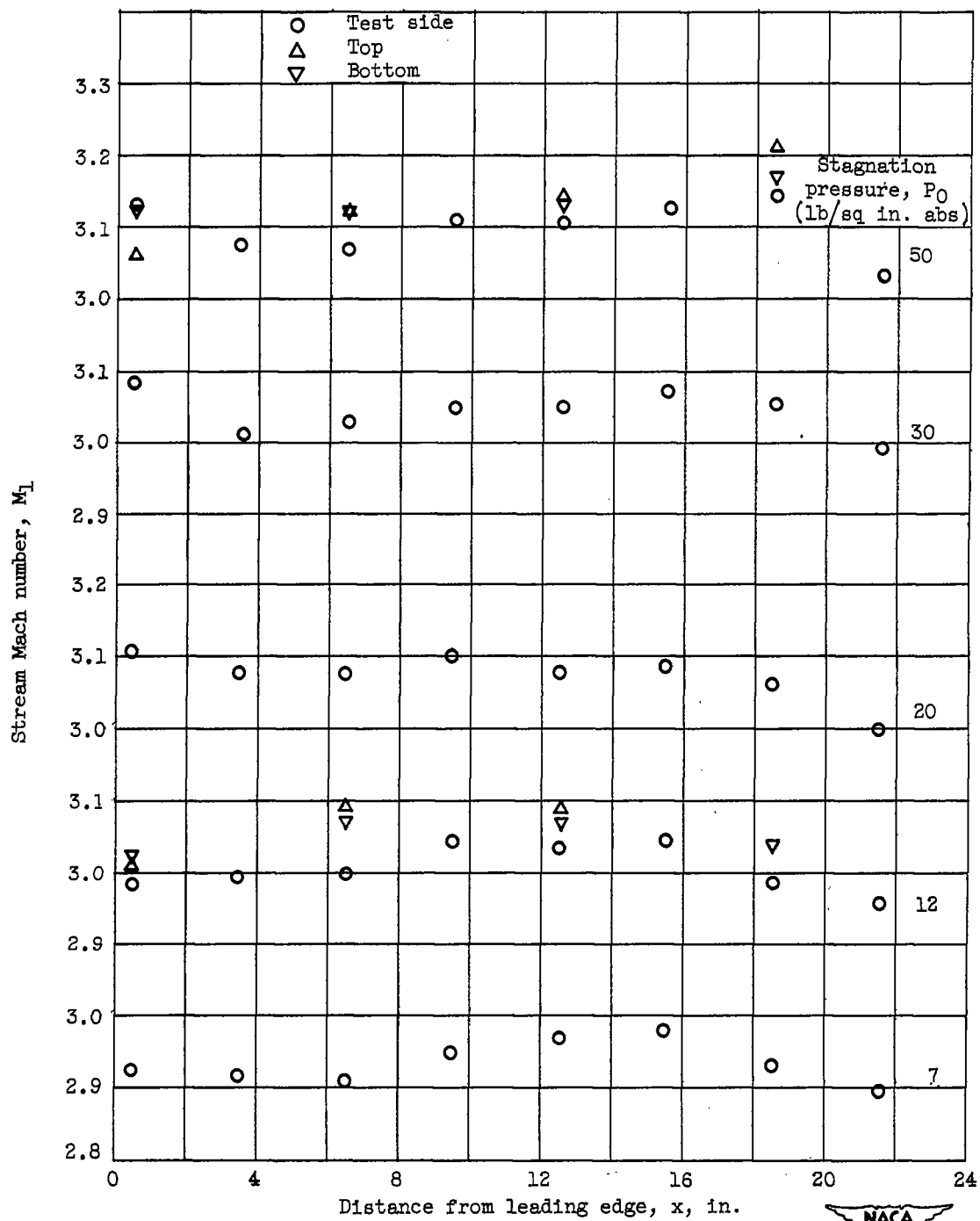
(a) Natural transition, 5-inch model.

Figure 4. - Mach number distributions.

2451
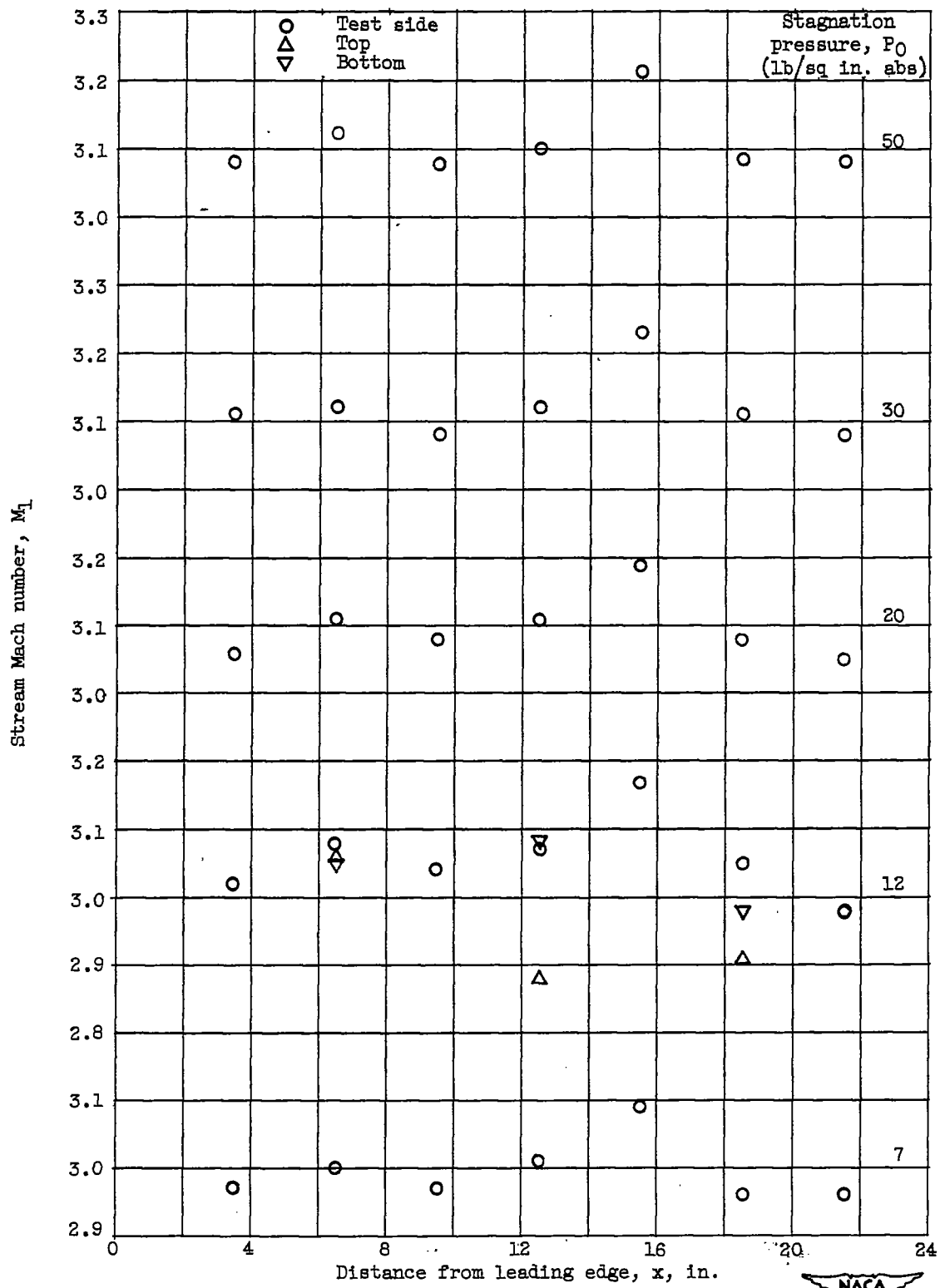
(b) Artificial transition, 5-inch model.

Figure 4. - Continued. Mach number distributions.
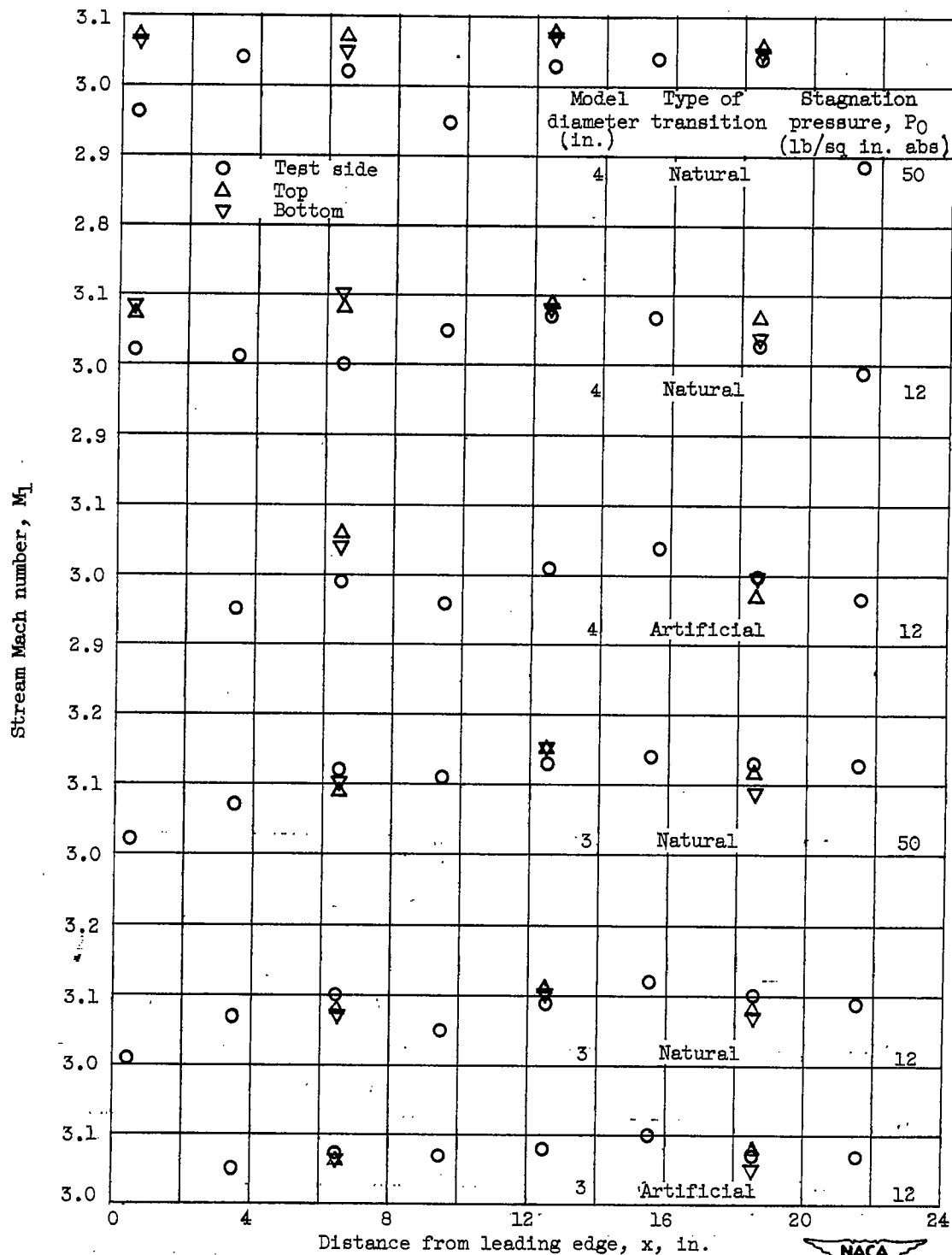
(c) Natural and artificial transition; 3- and 4-inch models.

Figure 4. - Concluded. Mach number distributions.
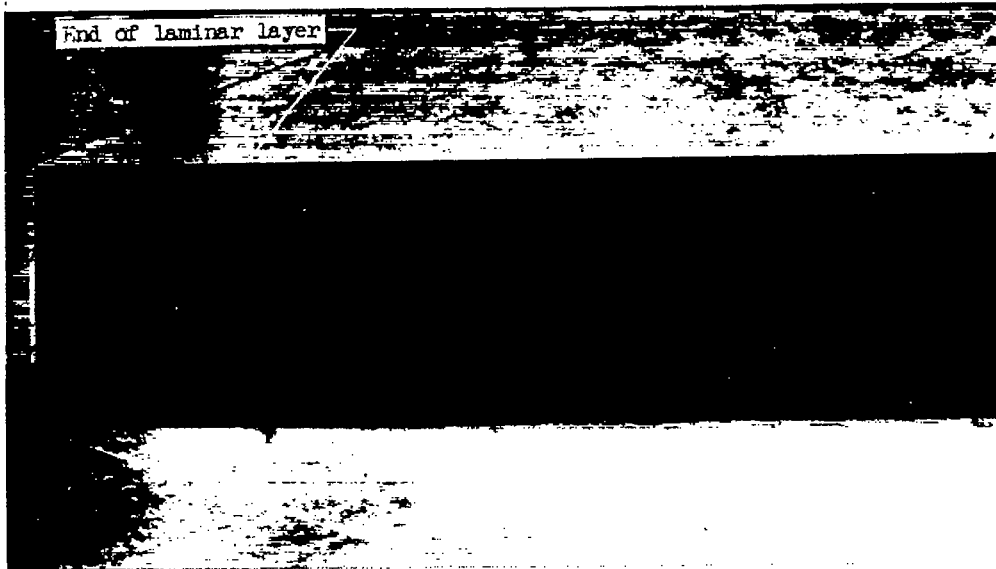
2451

(a) Natural transition.
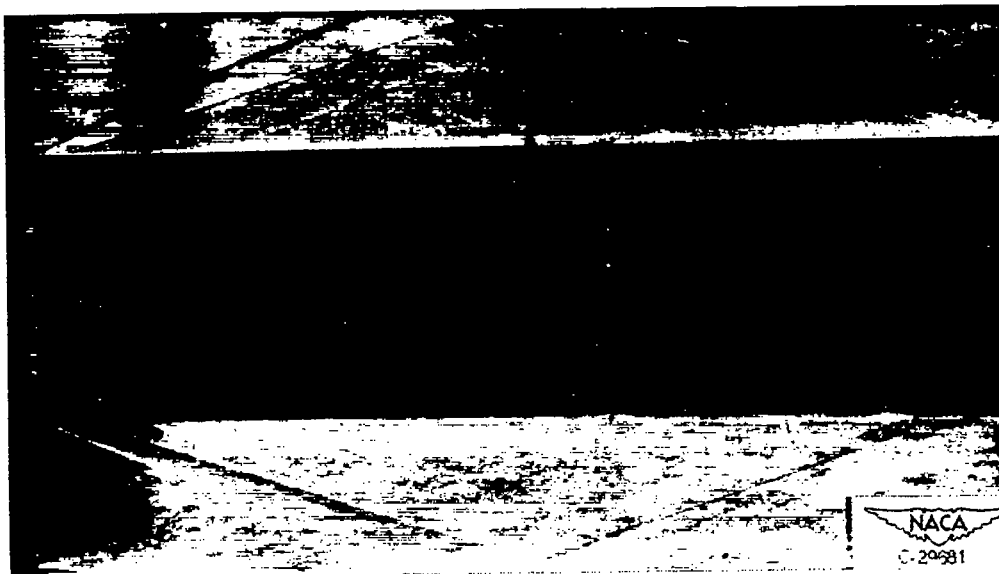
(b) Artificial transition. Stagnation pressure, 50 pounds per square inch absolute.

Figure 5. - Schlieren photograph of 5-inch model.
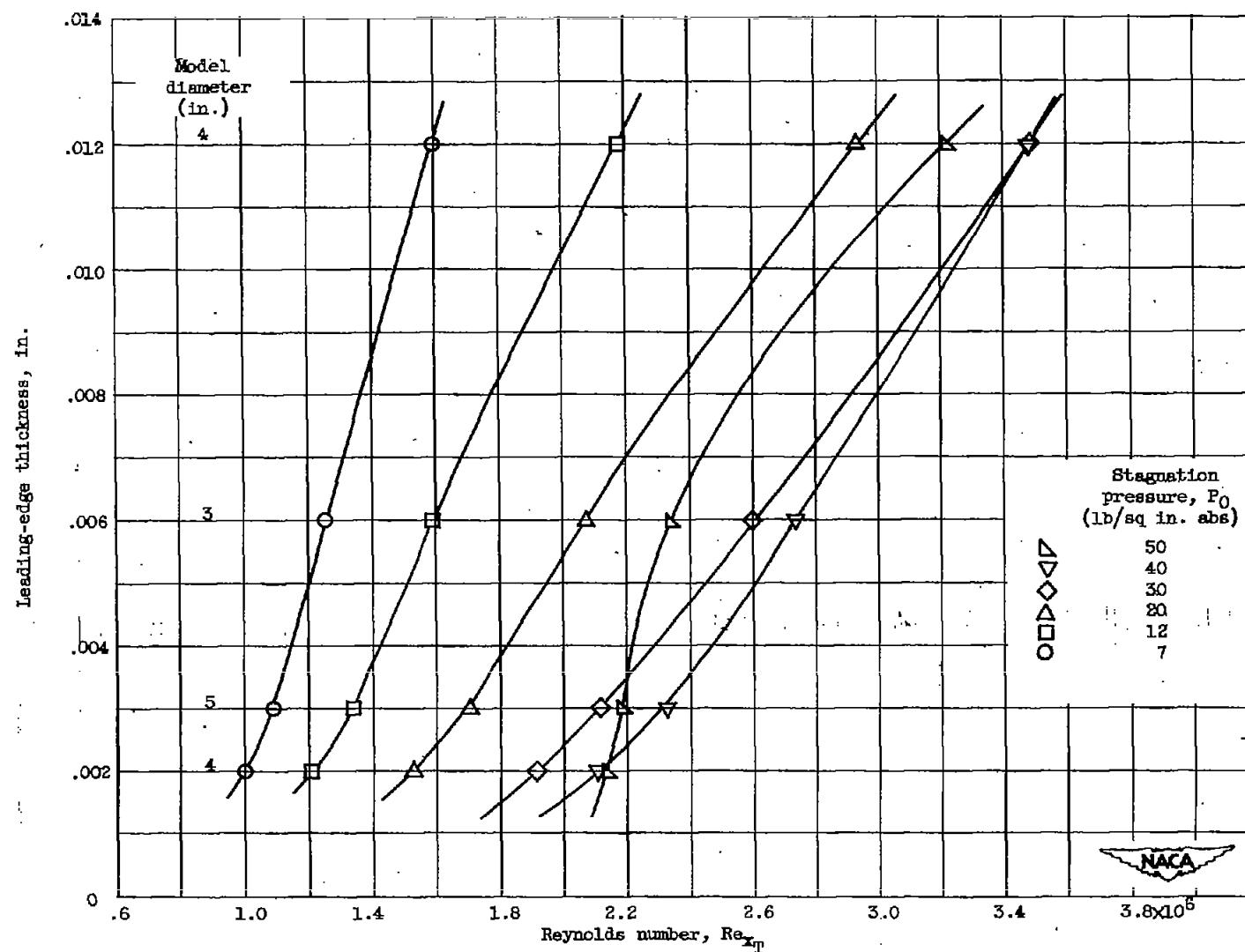
Figure 6. - Variation of transition Reynolds number with leading-edge thickness for all models.
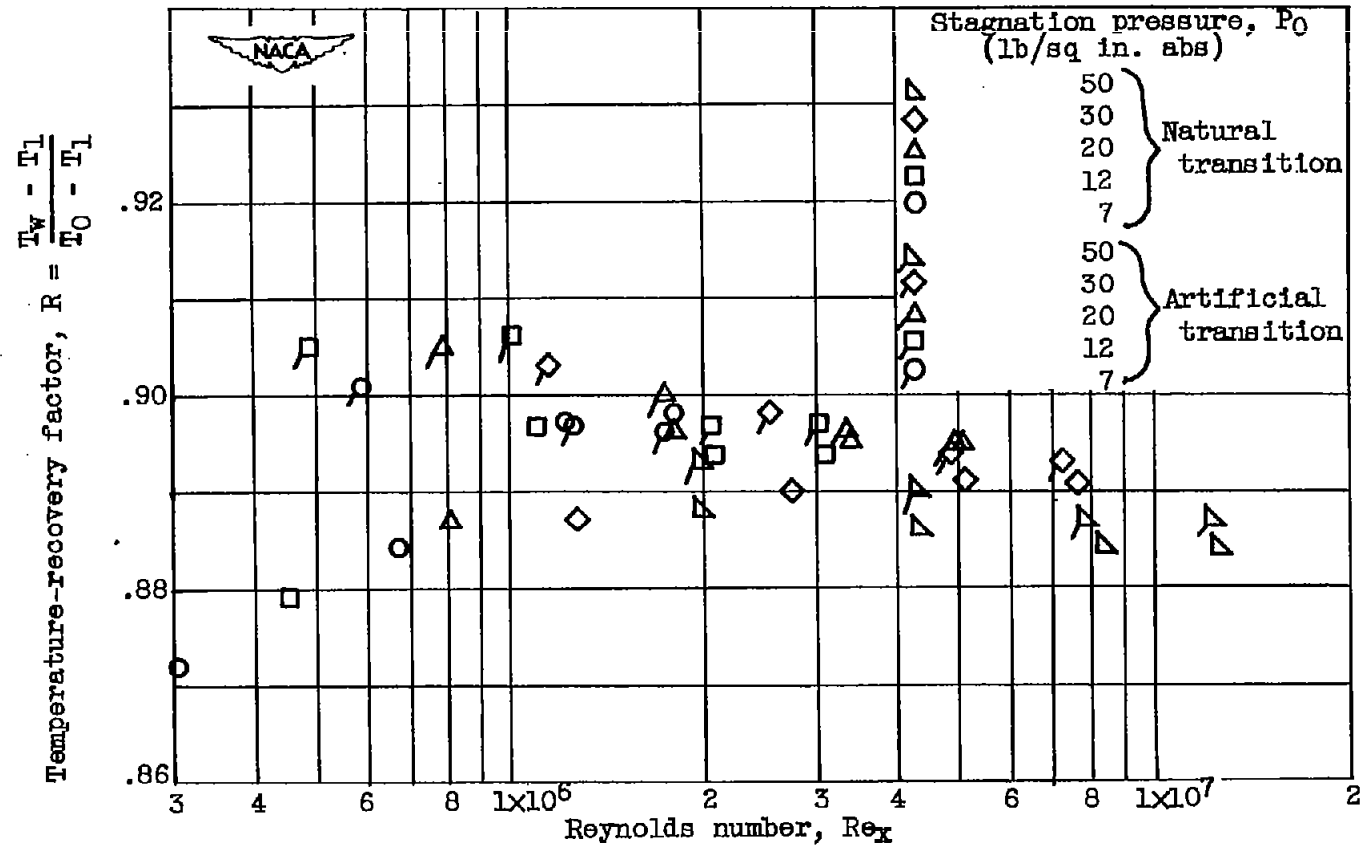
Figure 7. - Variation of recovery factor with Reynolds number.
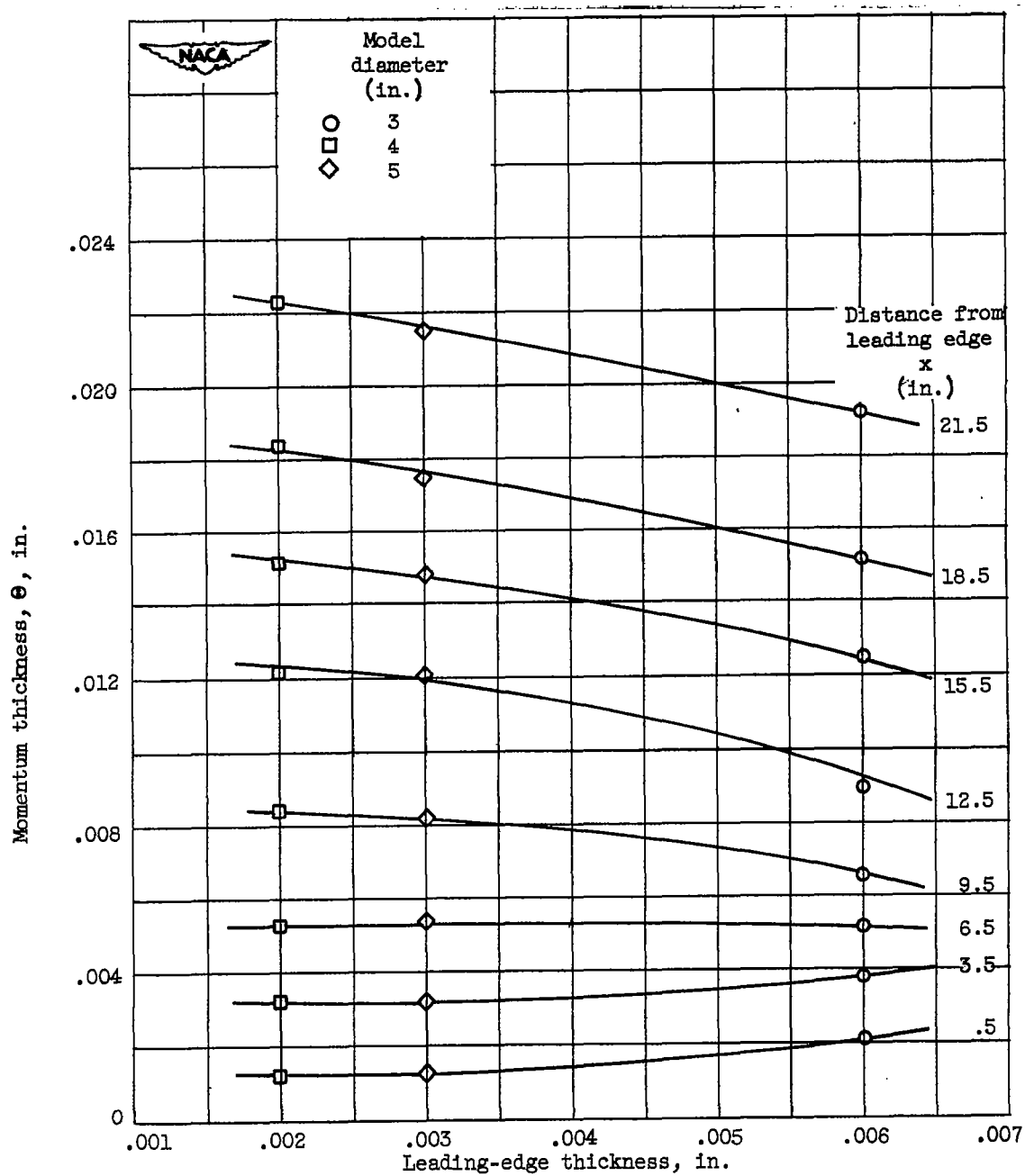
(a) Natural transition, stagnation pressure of 12 pounds
per square inch absolute.

Figure 8. - Effect of leading-edge thickness on momentum thickness.
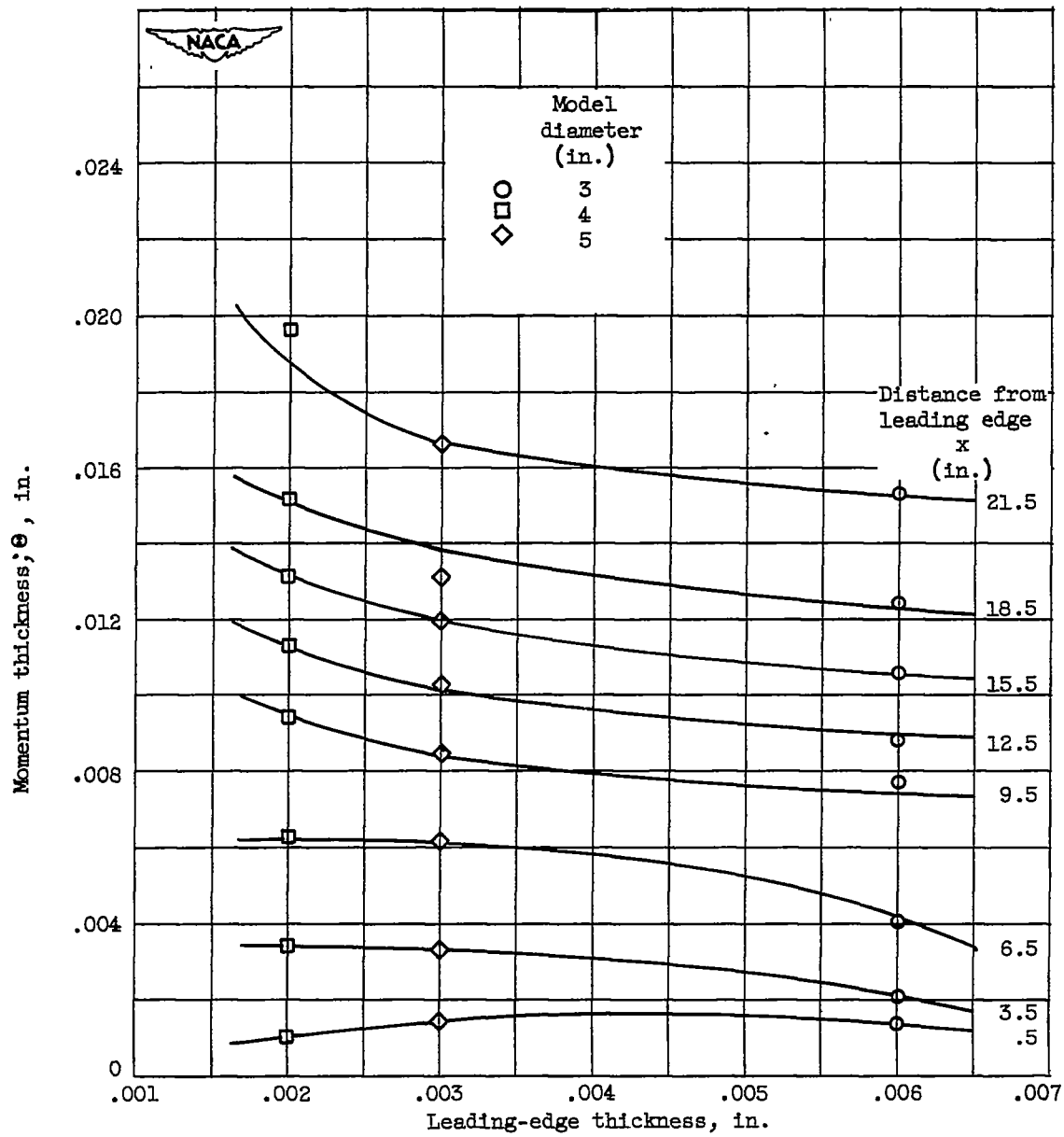
(b) Natural transition, stagnation pressure of 50 pounds
per square inch absolute.

Figure 8. - Continued. Effect of leading-edge thickness on momentum thickness.
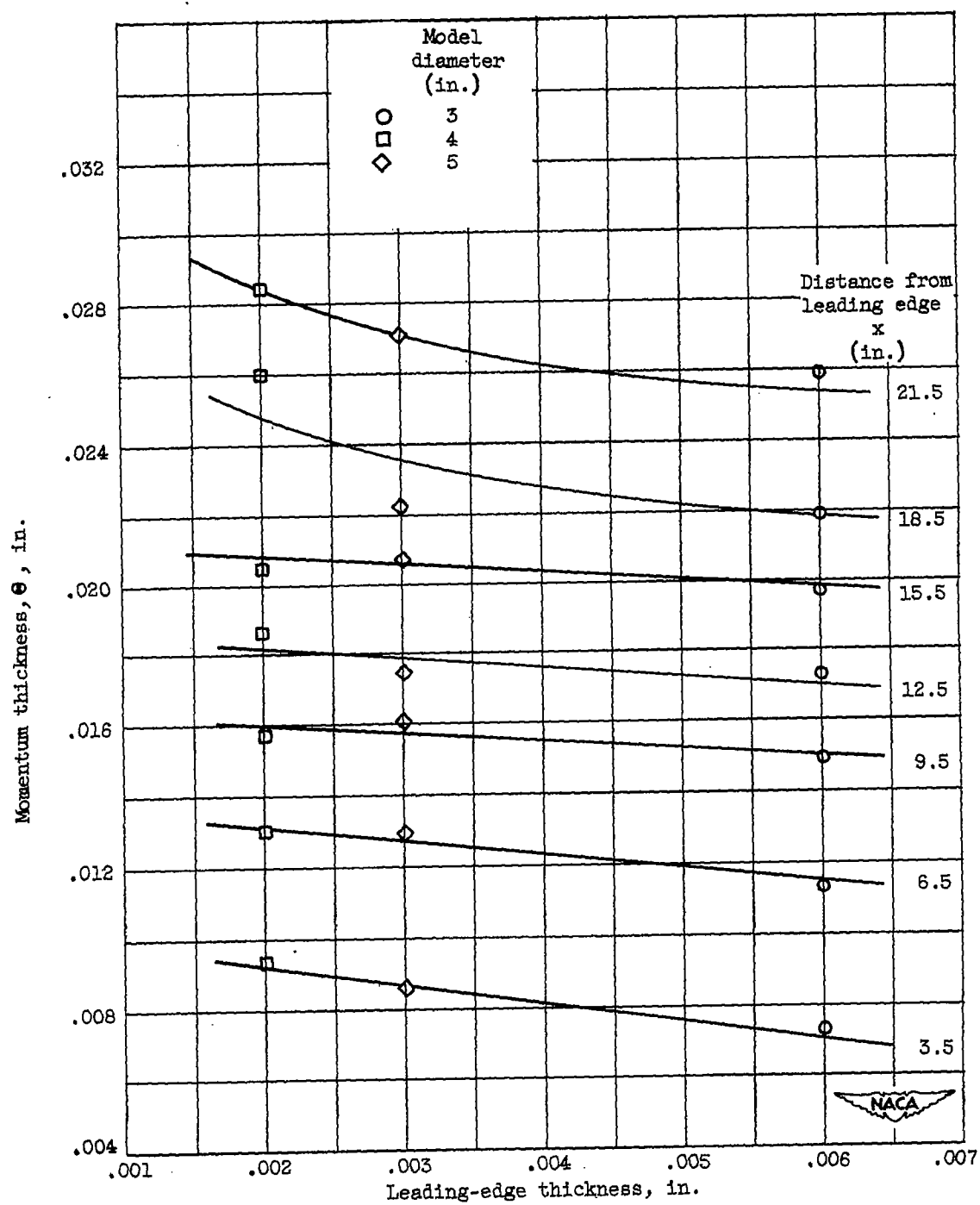
(c) Artificial transition, stagnation pressure of 12 pounds
per square inch absolute.

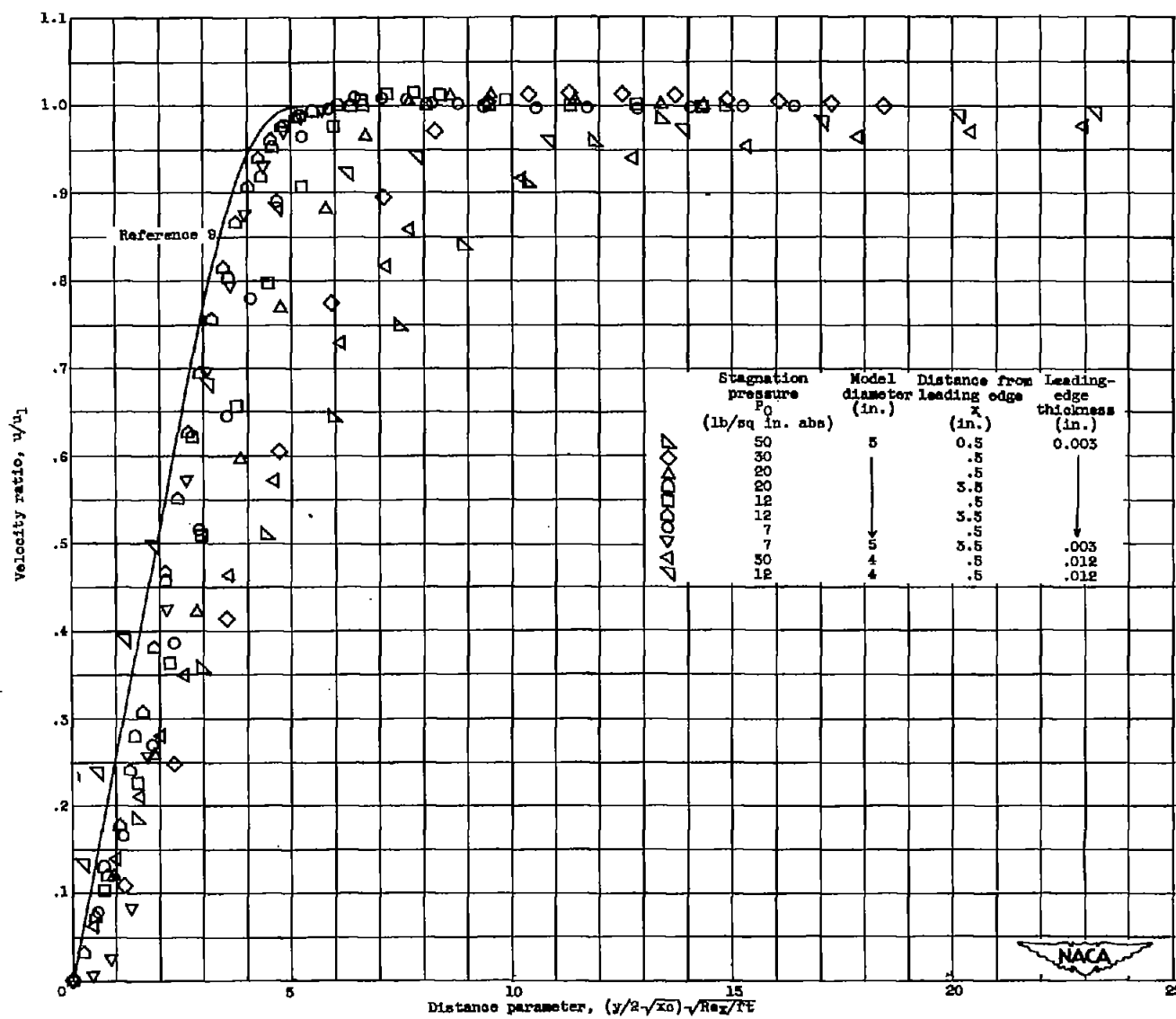Figure 8. - Concluded.   Effect of leading-edge thickness on momentum thickness.

Figure 9. - Laminar velocity profiles and comparison with theory. Side measurements.
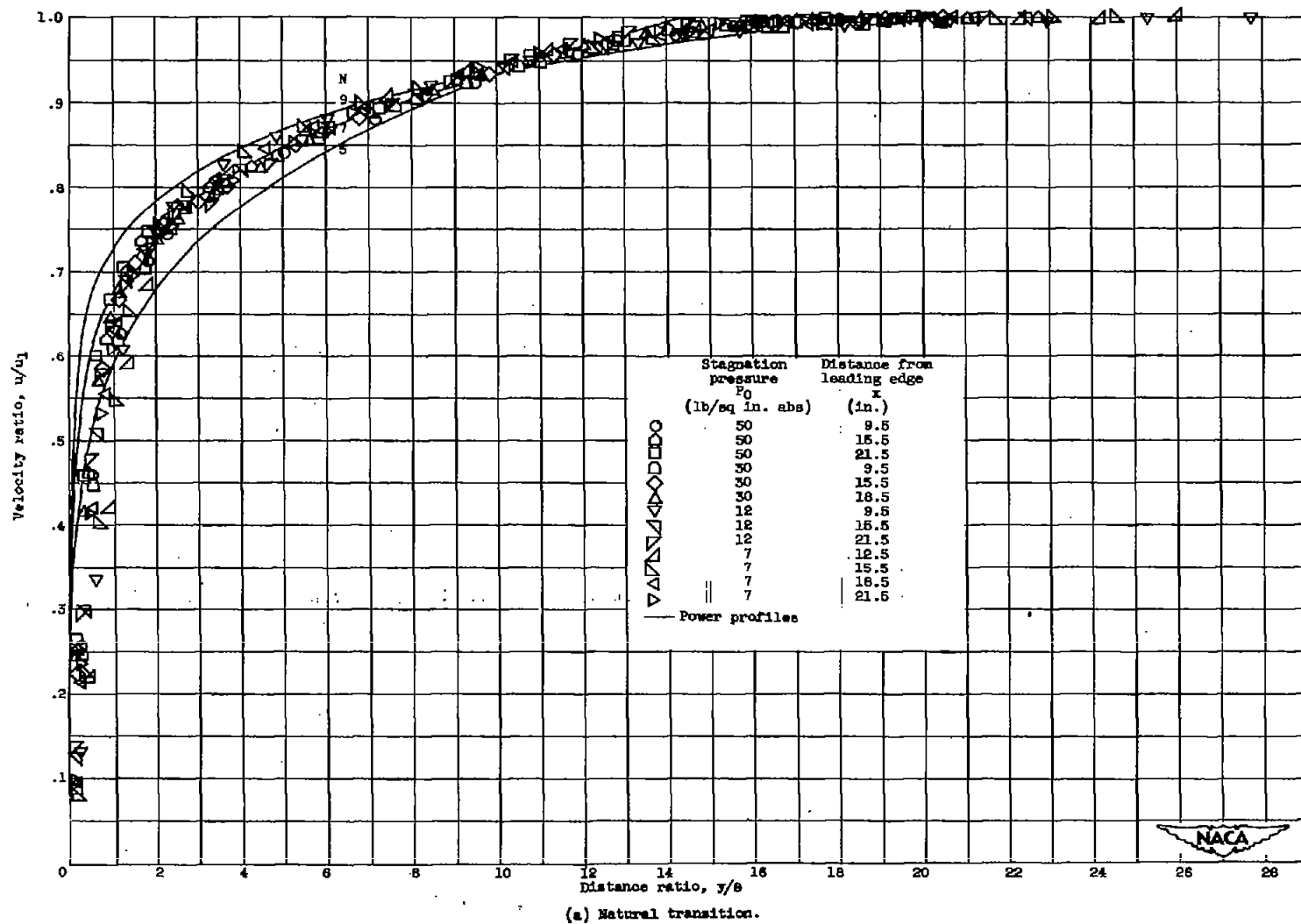
	Stagnation pressure P_0 (lb/sq in. abs)	Distance from leading edge x (in.)
○	50	9.5
◐	50	15.5
□	50	21.5
◇	30	9.5
✕	30	15.5
▽	30	18.5
◁	12	9.5
▷	12	15.5
▽	12	21.5
◁	7	12.5
‖	7	15.5
▷	7	18.5
▷	7	21.5
—— Power profiles		

(a) Natural transition.

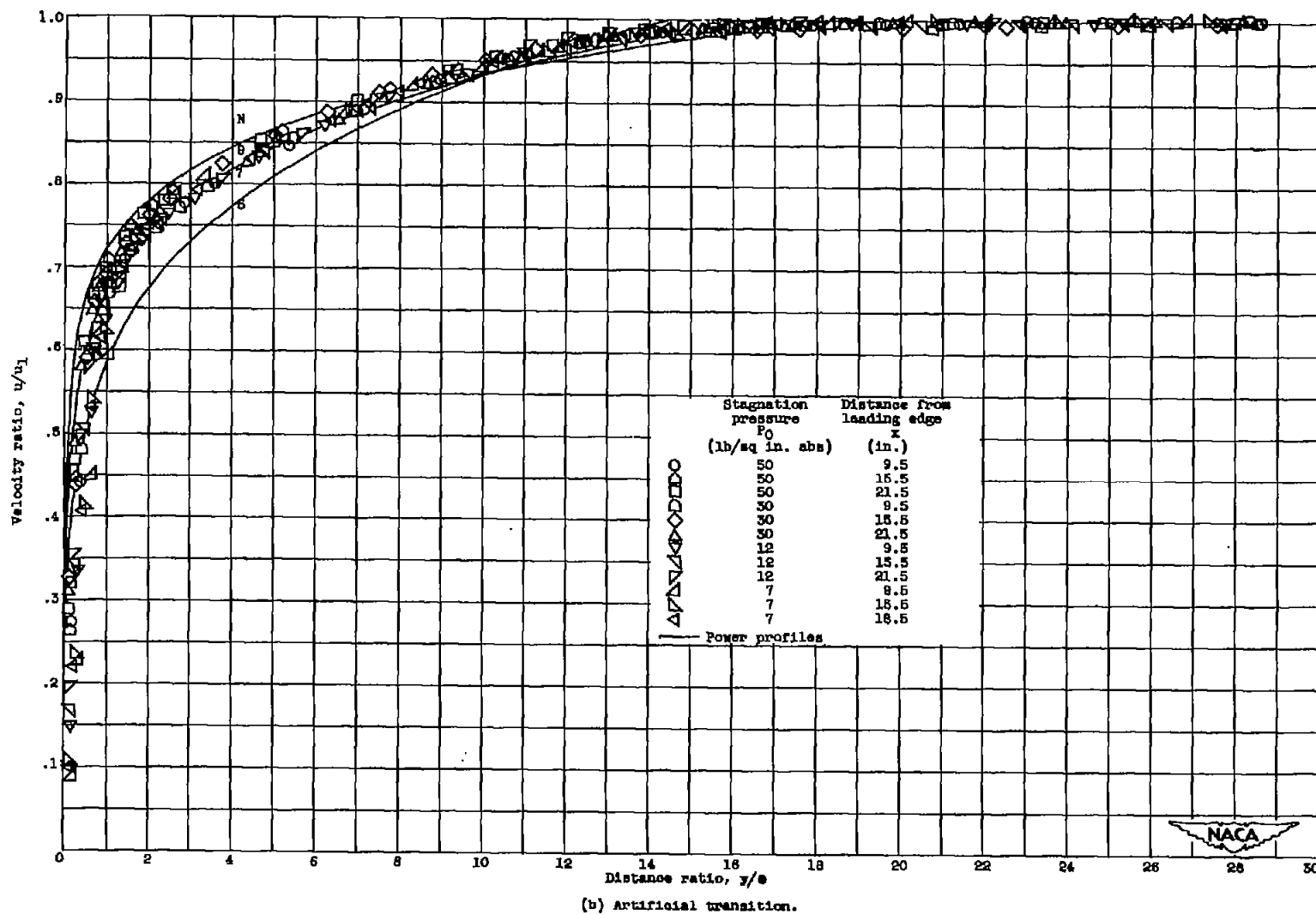Figure 10. – Turbulent velocity profiles and comparison with power profiles for 5-inch model. Side measurements.

Velocity ratio, u/h

	Stagnation pressure P_0 (lb/sq in. abs)	Distance from leading edge x (in.)
	50	9.5
	50	15.5
	50	21.5
	30	9.5
	30	15.5
	30	21.5
	12	9.5
	12	15.5
	12	21.5
	7	9.5
	7	15.5
	7	15.5
—— Power profiles		

Distance ratio, y/s

(b) Artificial transition.

Figure 10. - Concluded. Turbulent velocity profiles and comparison with power profiles for 5-inch model. Side measurements.
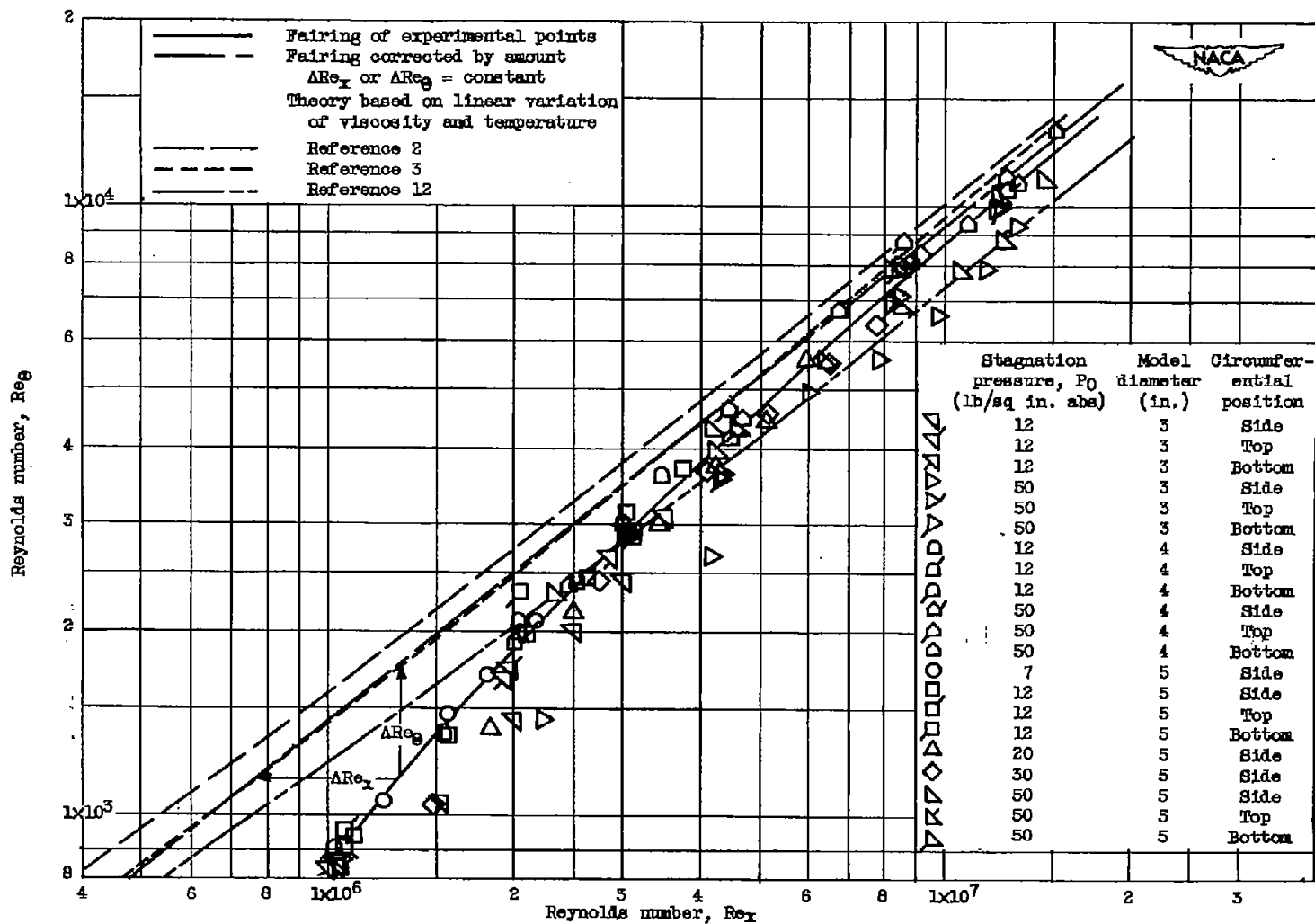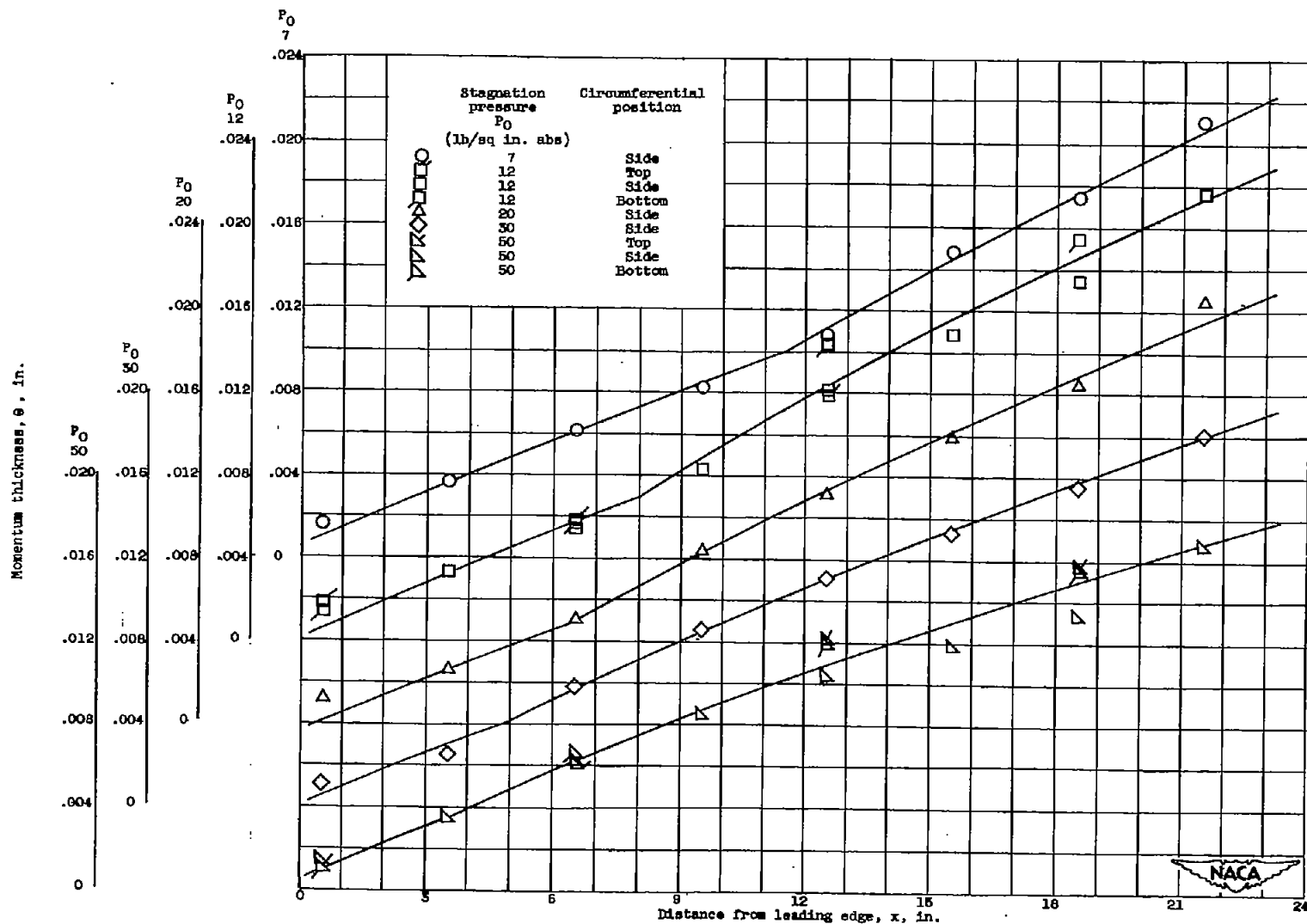
(a) Natural transition.

Figure 11. - Variation of Re_θ with Re_x for 3-, 4-, and 5-inch cylinder models and comparison with theory. Top, side, and bottom measurements.
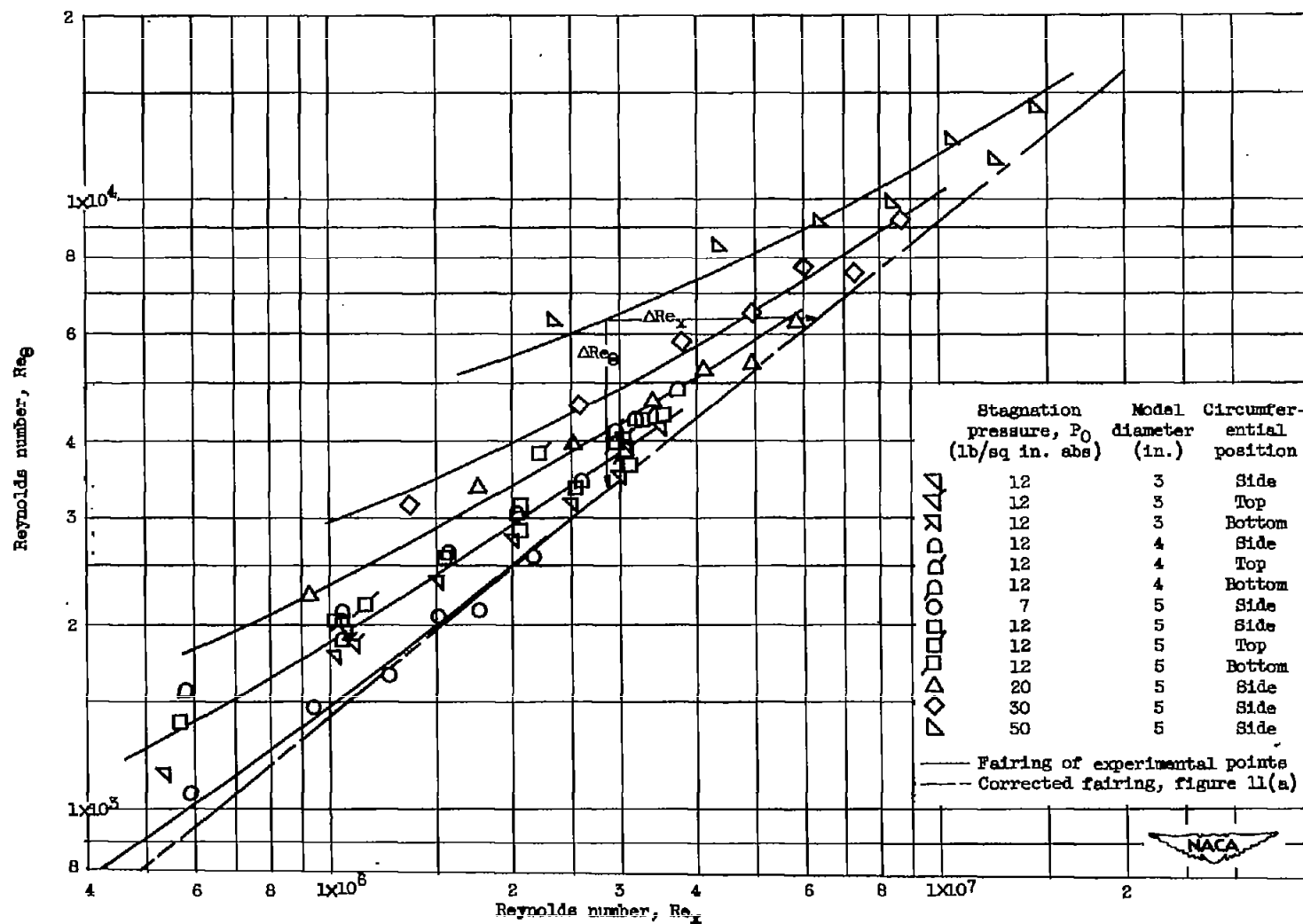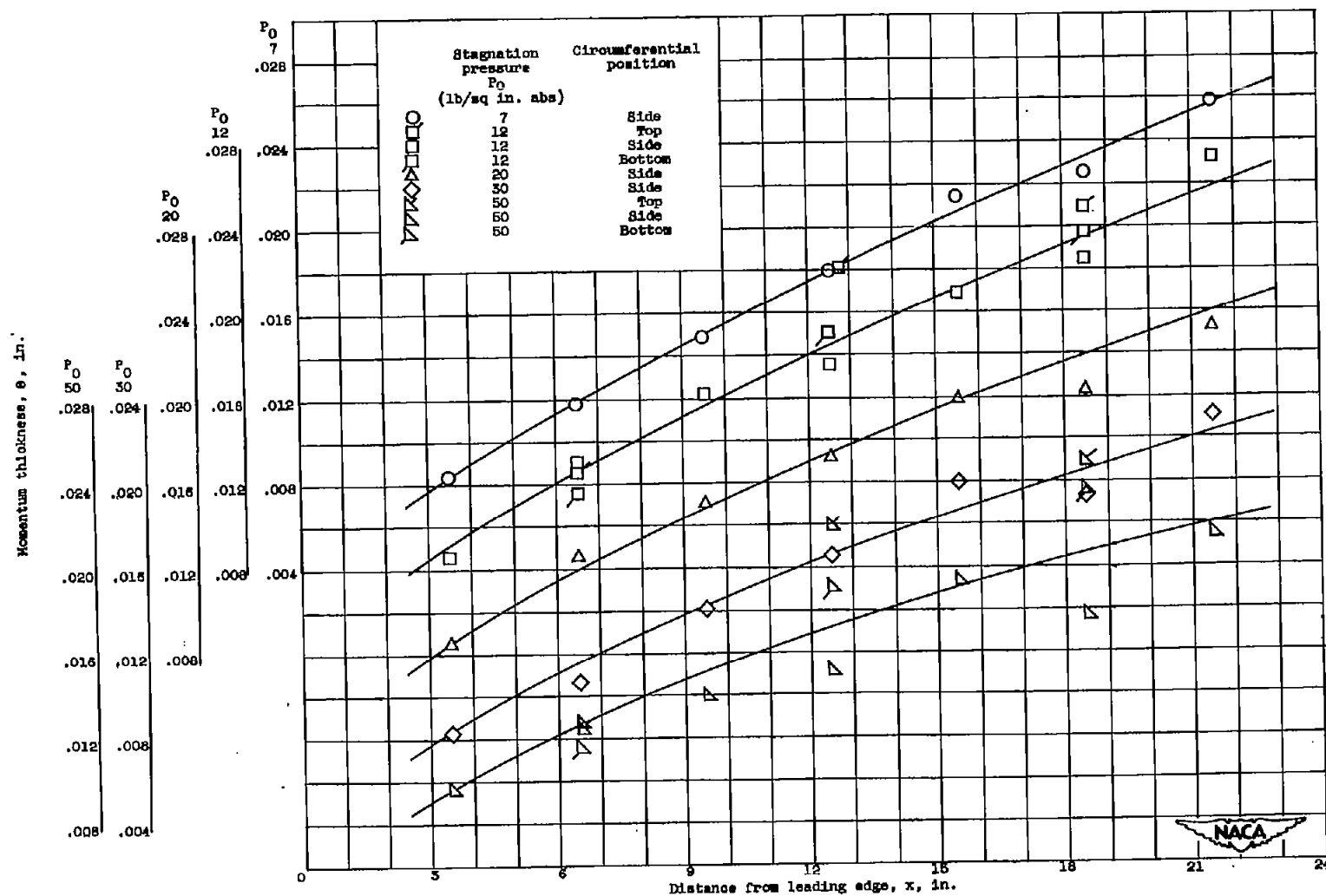
(b) Artificial transition.

Figure 11. - Concluded. Variation of Re_θ with Re_x for 3-, 4-, and 5-inch cylinder models and comparison with theory. Top, side, and bottom measurements.
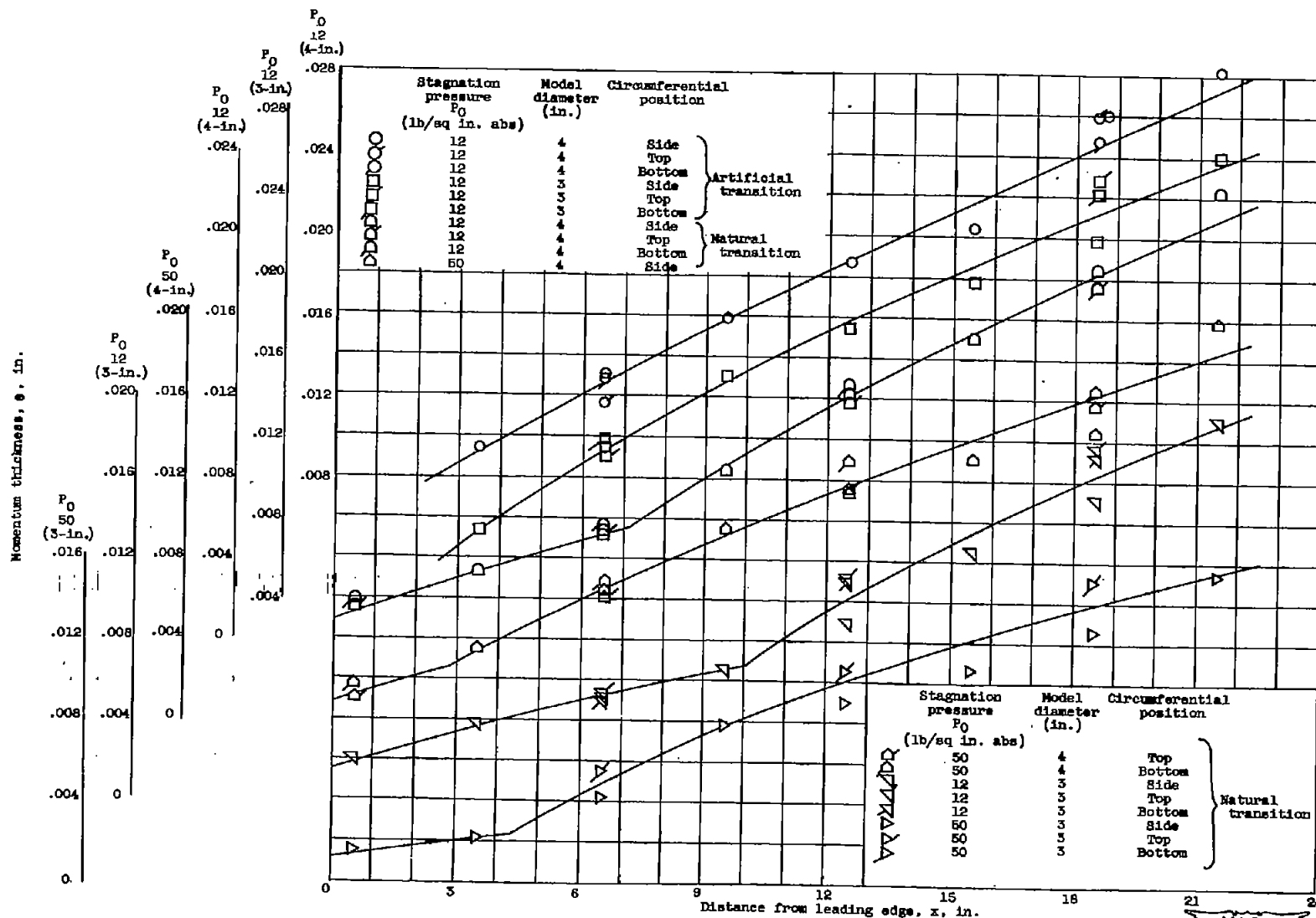
(a) Along 5-inch model, natural transition.

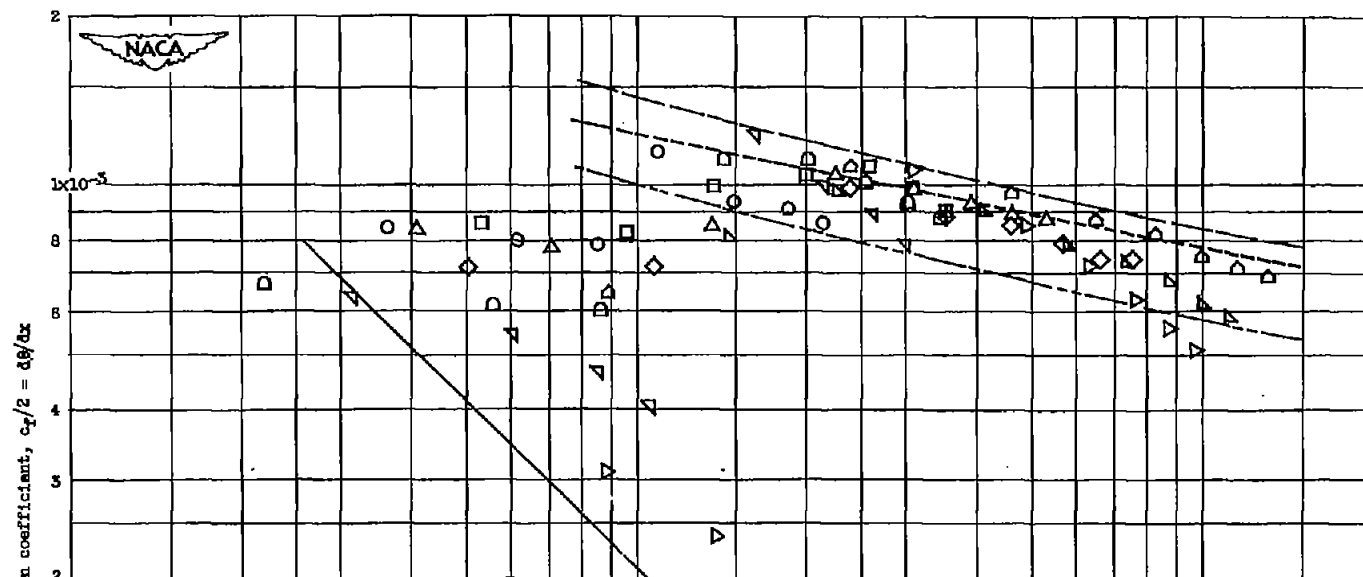Figure 12. - Momentum thickness distribution.

(b) Along 5-inch model, artificial transition.

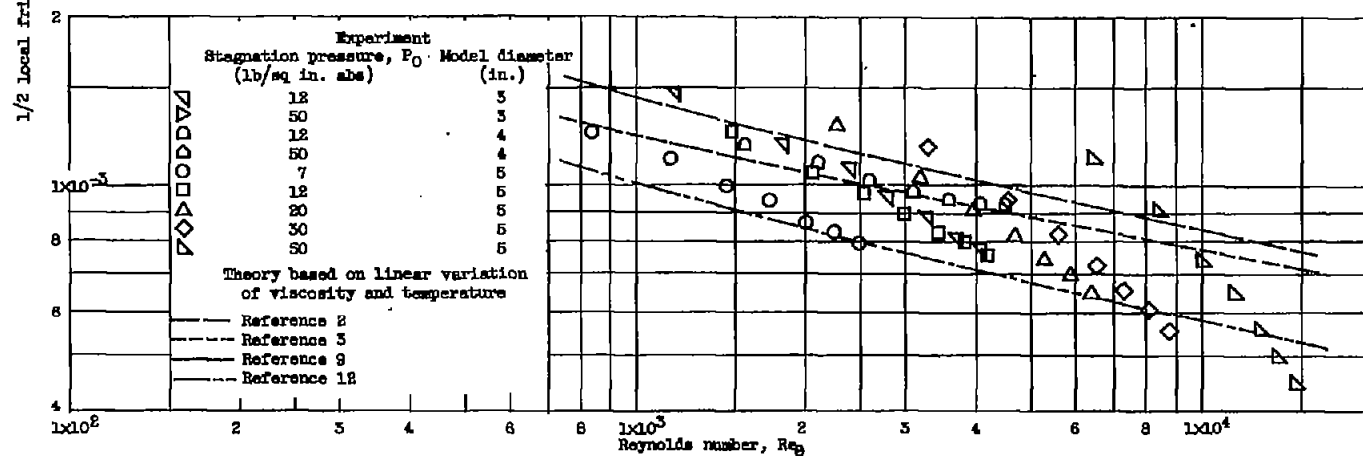Figure 12. - Continued. Momentum thickness distribution.

(a) Along 3- and 4-inch models, natural and artificial transition.

Figure 12. - Concluded. Momentum thickness distribution.

(a) Natural transition.

(b) Artificial transition.

Figure 15. - Variation of local friction coefficient with Re_θ for 3-, 4-, and 5-inch models.
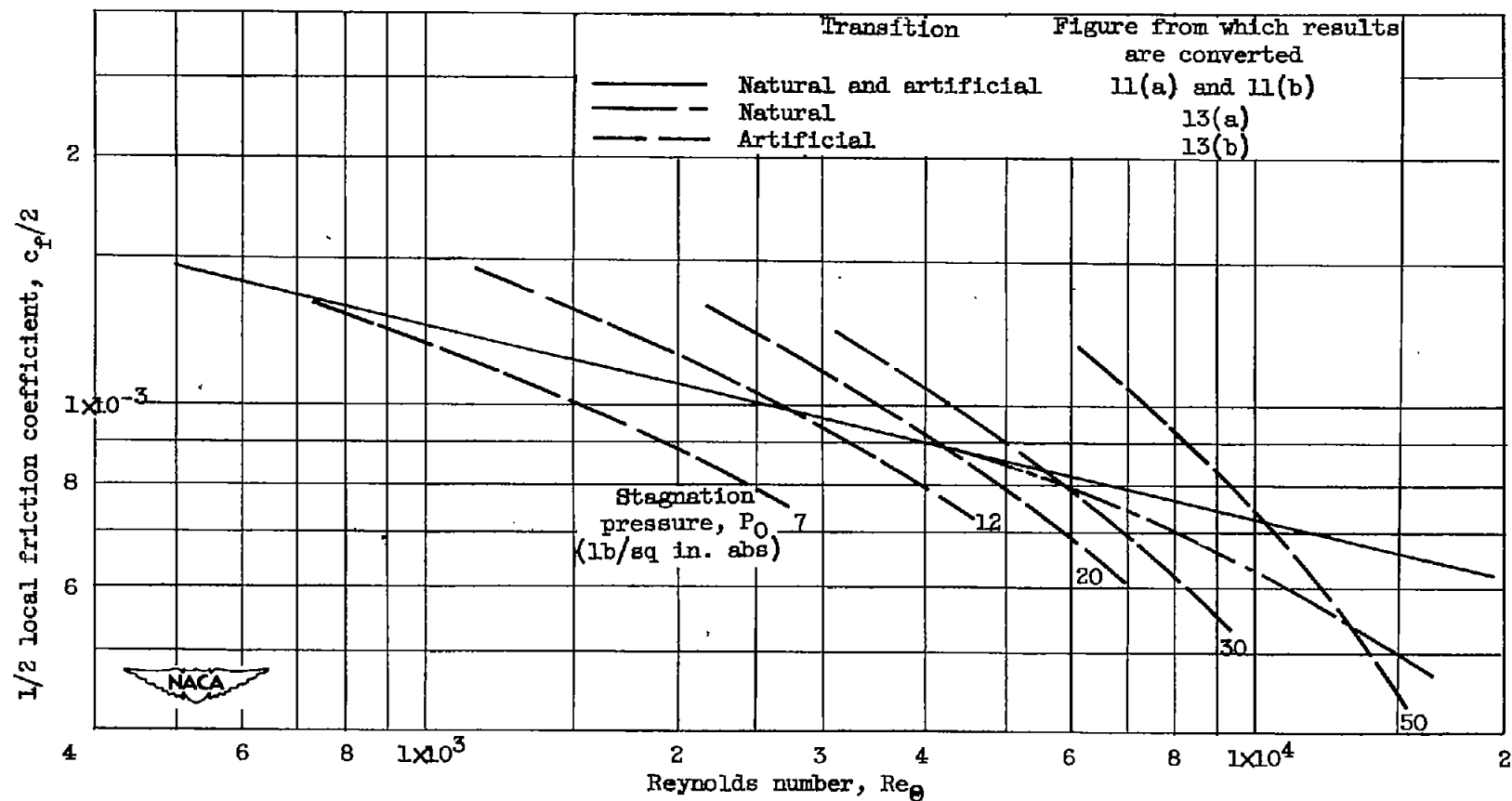
Figure 14. - Summary of measured friction coefficients as function of Re_θ on 3-, 4-, and 5-inch models. Natural and artificial transition.

Experiment

Stagnation pressure p_0 (lb/sq in. abs)	Distance from leading edge x (in.)	1/2 local friction coefficient $c_f/2$
50	9.5	0.00075
50	15.5	.00071
50	21.5	.00074
30	9.5	.00087
30	15.5	.00078
30	18.5	.00075
12	9.5	.00118
12	15.5	.00102
12	21.5	.00088
7	12.5	.00134
7	15.5	.00125
7	18.5	.00117
7	21.5	.00120

Theory

------- Reference 10, laminar sublayer
——— Reference 10, incompressible turbulent flow
— — Reference 11, compressible turbulent flow, $M_1 = 3.05$; $c_f/2 = 0.00072$
——— Reference 11, compressible turbulent flow, $M_1 = 3.05$; $c_f/2 = 0.00125$

Velocity parameter, $u^+ = \dfrac{u}{\sqrt{\tau_0/\rho}} = \dfrac{u}{u_1}\sqrt{\left(\dfrac{\rho}{\rho_1}\right)\left(\dfrac{2}{c_f}\right)}$

Distance parameter, $\log y^+ = \log \dfrac{y\sqrt{\tau_0/\rho}}{\nu} = \log \dfrac{u_1 y}{\nu}\sqrt{\left(\dfrac{\rho_1}{\rho}\right)\left(\dfrac{c_f}{2}\right)}$
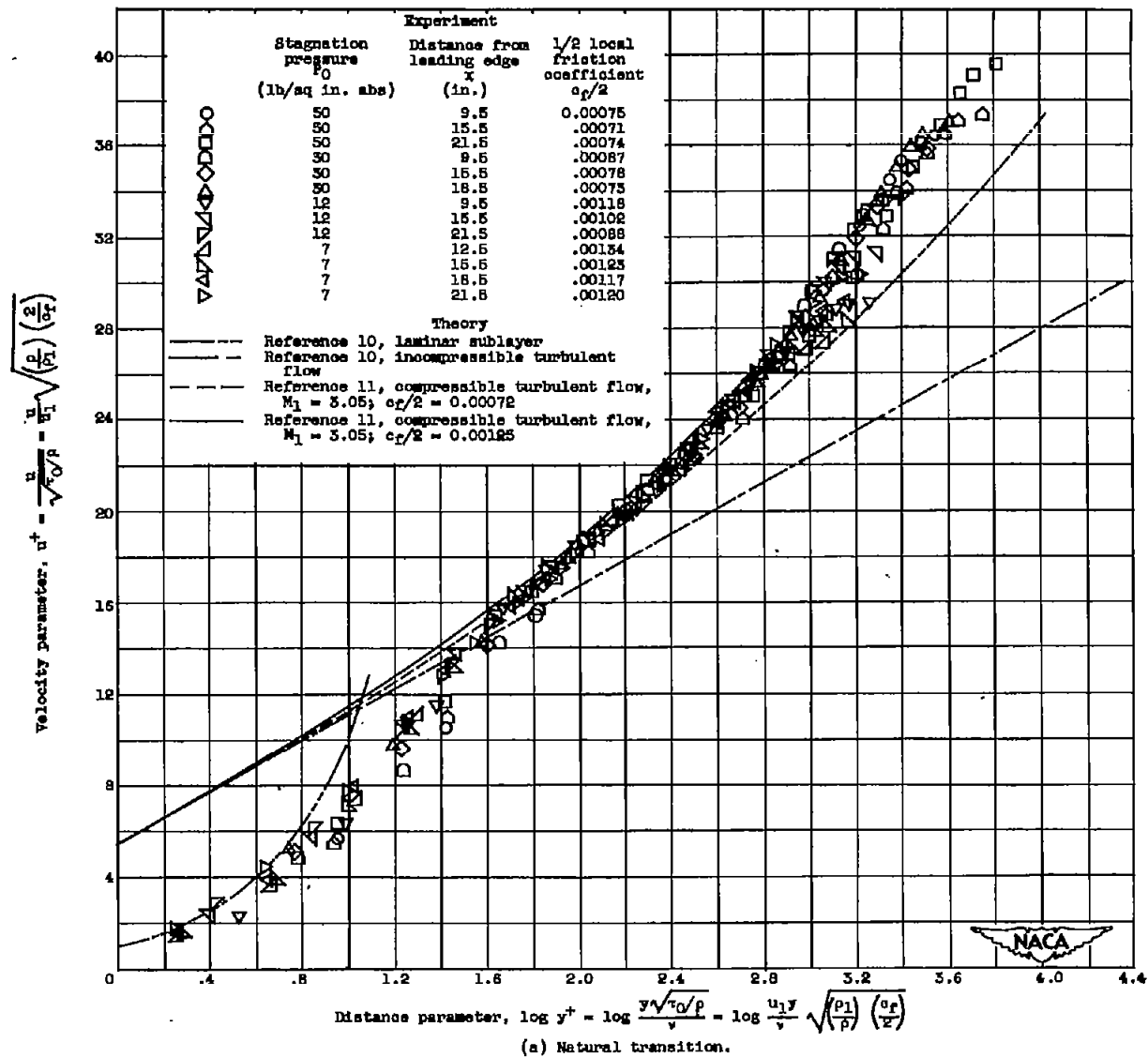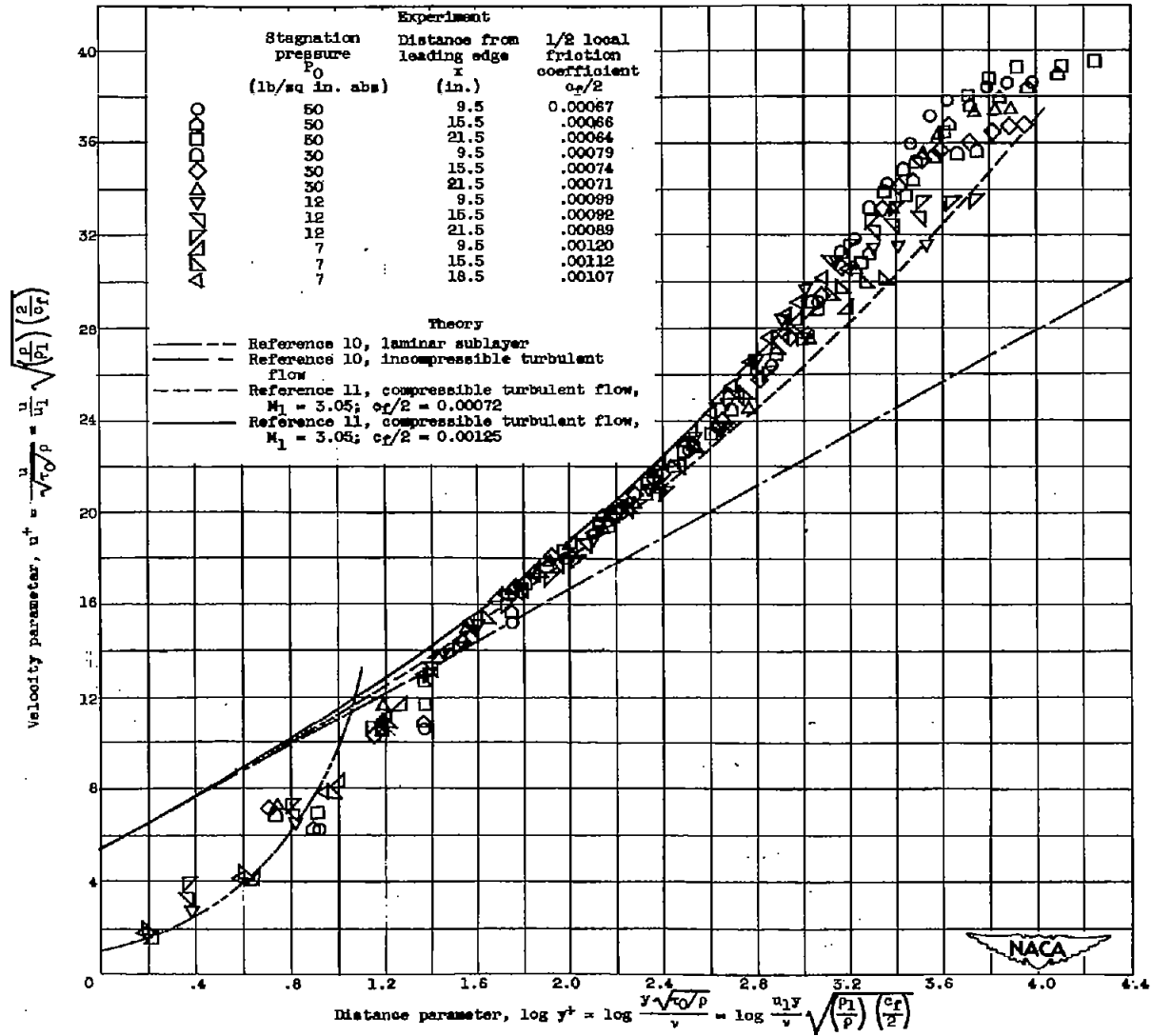
NACA

(a) Natural transition.

Figure 15. - Turbulent velocity profiles and comparison with theory. 5-inch model, side measurements.

(b) Artificial transition.

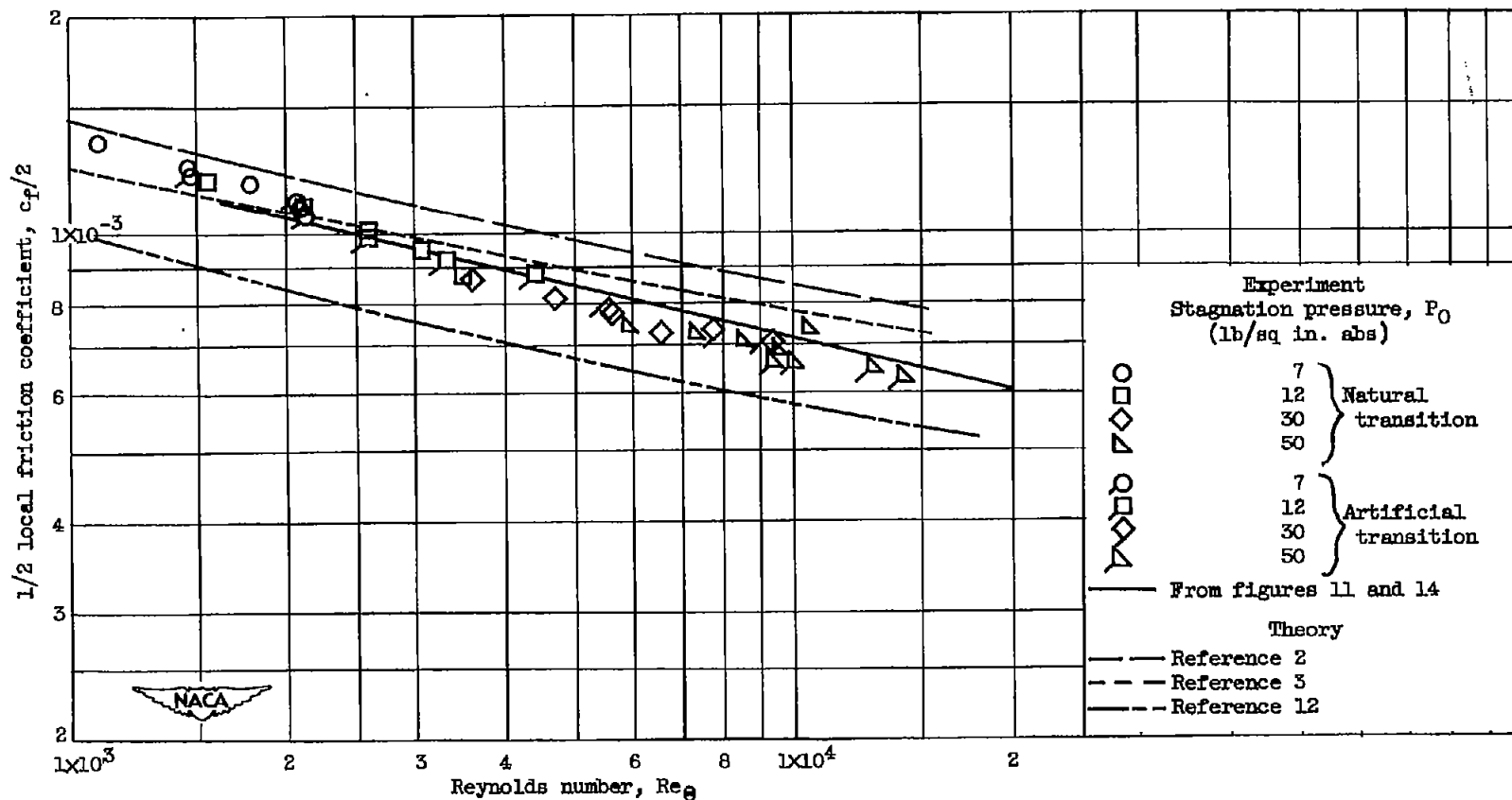Figure 15. - Concluded. Turbulent velocity profiles and comparison with theory. 5-inch model, side measurements.

Figure 16. - Corrected measured friction coefficients as function of Re_θ on 5-inch model. Natural and artificial transition.